Max-Planck-Institut für Meteorologie
Max Planck Institute for Meteorology

MAX-PLANCK-GESELLSCHAFT

Effect of Daily Surface Flux Anomalies on the Time-Mean Oceanic Circulation

Balan Sarojini Beena

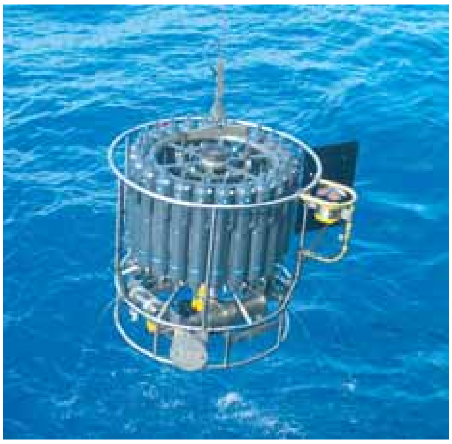

Berichte zur Erdsystemforschung 31/2006

Reports on Earth System Science

Hinweis

Die Berichte zur Erdsytemforschung werden vom Max-Planck-Institut für Meteorologie in Hamburg in unregelmäßiger Abfolge herausgegeben.

Sie enthalten wissenschaftliche und technische Beiträge, inklusive Dissertationen.

Die Beiträge geben nicht notwendigerweise die Auffassung des Instituts wieder.

Die "Berichte zur Erdsystemforschung" führen die vorherigen Reihen "Reports" und "Examensarbeiten" weiter.

Notice

The Reports on Earth System Science are published by the Max Planck Institute for Meteorology in Hamburg. They appear in irregular intervals.

They contain scientific and technical contributions, including Ph. D. theses.

The Reports do not necessarily reflect the opinion of the Institute.

The "Reports on Earth System Science" continue the former "Reports" and "Examensarbeiten" of the Max Planck Institute.

Anschrift / Address

Max-Planck-Institut für Meteorologie
Bundesstrasse 53
20146 Hamburg
Deutschland

Tel.: +49-(0)40-4 11 73-0
Fax: +49-(0)40-4 11 73-298
Web: www.mpimet.mpg.de

Layout:

Bettina Diallo, PR & Grafik

Titelfotos:
vorne:
Christian Klepp - Jochem Marotzke - Christian Klepp
hinten:
Clotilde Dubois - Christian Klepp - Katsumasa Tanaka

Berichte zur Erdsystemforschung 31/2006

Effect of Daily Surface Flux Anomalies on the Time-Mean Oceanic Circulation

Dissertation zur Erlangung des Doktorgrades der Naturwissenschaften
im Departement Geowissenschaften der Universität Hamburg
vorgelegt von

Balan Sarojini Beena
aus Kerala, Indien

Hamburg 2006

Reports on Earth System Science 31/2006

ISSN 1614-1199

Balan Sarojini Beena
Max-Planck Institut für Meteorologie
Bundesstr. 53
20146 Hamburg
Germany

Als Dissertation angenommen
vom Departement Geowissenschaften der Universität Hamburg

auf Grund der Gutachten von
Prof. Dr. Detlef Quadfasel
und
Dr. Jin-Song von Storch
Hamburg, den 10. November 2006
Professor Dr. Kay-Christian Emeis
Leiter des Departements für Geowissenschaften

ISSN 1614-1199

Effect of Daily Surface Flux Anomalies on the Time-Mean Oceanic Circulation

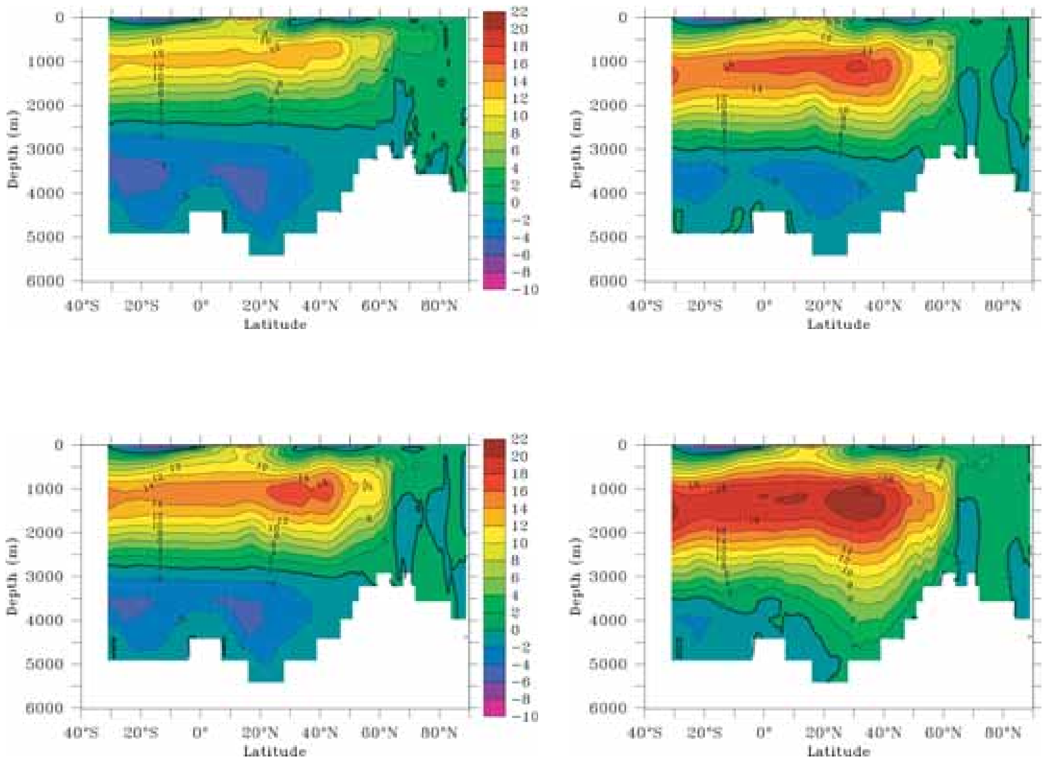

Atlantic Meridional Overturning Circulation (Sv)

Balan Sarojini Beena

Hamburg 2006

CONTENTS

Abstract

Previous studies suggest that the global meridional overturning circulation is driven or strongly affected by small-scale diapycnal mixing, large-scale wind-driven upwelling and mean surface bouyancy fluxes. This thesis studies the role of a fourth factor, namely the daily flux anomalies of momentum, heat and freshwater at the sea surface, in determining the overturning circulation.

The effect of daily flux anomalies is studied using an empirical flux model. The model produces fluctuating fluxes resulting from the oceanic feedbacks on the fluxes and from the atmospheric turbulence. The model is able to respond to sea surface conditions such as Polynya and El-Niño. It captures different air-sea interaction processes suggested by cross-correlation functions. The magnitude and spatial characteristics of the flux anomalies are comparable to those produced by an atmospheric general circulation model (GCM) of a coupled atmosphere-ocean GCM.

Various experiments are carried out by driving an ocean general circulation model with different terms in the empirical model. It is found that daily flux anomalies significantly alter the meridional overturning circulation (MOC) and the Antarctic circumpolar current (ACC). Flux anomalies lead to an increase in the MOC of about 4 Sv and a decrease in the ACC of about 65 Sv. These changes are approximately 30% of the MOC and ACC obtained without daily flux anomalies. They are caused partly by setting a realistic 3-dimensional density distribution via the SST-feedback inherent in the daily fluxes, and partly by providing additional vertical mixing via fluctuating flux forcing.

The latter effect is novel. Due to the non-linear nature of convection, fluctuating buoyancy anomalies tend to increase convective mixing in mostly stable regions and to decrease convective mixing in mostly unstable regions.

As a result, global-scale changes in the mixing structure in the ocean are found. To conclude, the results of the experiments suggest that both the oceanic feedback and atmospheric fluctuating part of the daily flux anomalies play an essential role in determining the time-mean circulation in the ocean.

1. INTRODUCTION

The global meridional overturning circulation (MOC) of the ocean plays a crucial role in the earth's climate. Hence, it is a matter of concern for the society, ecosystem and economy of our world. Any change in the MOC, regardless of natural or anthropogenic origin, can considerably affect global climate through the world-wide ocean conveyor belt and complex ocean-atmosphere interactions. Understanding how our climate varies over decades or how it changes over the next century is difficult without a deep understanding of the mechanisms determining the present-day MOC.

The issue of what determines the strength of the MOC has hence drawn the attention of many researchers. By and large, there exist two directions concerning the factors which control the MOC. One focuses on the mean buoyancy forcing at the sea surface. The surface buoyancy forcing affects the surface density and from that the site and intensity of the deep water formation, i.e. the conversion of surface water masses to deep waters by raising their density through cooling and/or increasing salinity. The deep water formation constitutes the downward branch of the Atlantic MOC. The controlling role in determining the deep water formation makes the *surface buoyancy forcing* crucial for the stability of the MOC (Rahmstorf, 1995).

The second direction originates from the physical modeling study by Sandström (1908). It focuses on the mechanisms which are able to bring the densy deep water to the surface and deals therefore mainly with the upward branch of the MOC. Sandström conducted a series of physical experiments by placing sources of heating and cooling at opposite sides of a water tank and changed their relative depths alternatively to higher, equal or lower. He found that when heating and cooling occur at the surface, or when cooling occurs at a lower depth than that of heating, there was no significant overturning circulation. In other words, a steady, deep overturning circulation is only possible when heating occurs at a lower depth than cooling, which is known as the Sandström's theorem. This theorem implies that surface buoyancy fluxes alone cannot drive the overturning circulation in the ocean and points to other sources of energy within the ocean to bring dense deep water up.

Subsequent research found that turbulent mixing in the ocean interior is a source of energy to bring dense deep water up across the stratification in the ocean. Munk and Wunsch (1998) confirmed the role of *turbulent mixing* of heat as the energy source that lightens water masses in the deep ocean and causes them to rise. They suggested that the diapycnal mixing i.e. mixing across density layers, is caused by the breaking of internal waves in the interior of the ocean due to winds and tides in interaction with bottom topography. Based on the available measurements of mixing in the ocean, they estimated the energy required to sustain the overturning circulation.

The studies initiated by Toggweiler and Samuels (1995) led to a contrasting view of the role of Southern Ocean winds on the MOC. Toggweiler and Samuels (1993) detected North Atlantic deep water in near-surface Southern Ocean waters. Following this observational evidence, Toggweiler and Samuels (1995) showed numerically that the westerly winds over the Southern Ocean caused northward Ekman transport, which increased the southward return flow of the MOC via the northern North Atlantic. The latitude band of the Drake Passage has no longitudinal topographic borders down to a depth of about 2500m so that no zonal pressure gradient and hence no meridional geostrophic flow can be built up at these depths and latitudes leading to the so-called "Drake Passage Effect". Toggweiler and Samuels (1995) argued that the return flow of the MOC is maintained gestrophically by zonal pressure gradients at the depth of two under-sea topographic features. According to them, stronger *wind stress* over the Southern Ocean caused stronger MOC and stronger wind-driven upwelling of deep water in the Antarctic circumpolar current (ACC) region. The importance of wind-driven upwelling in the Southern Ocean is also emphasized in the energy estimate by Webb and Suginohara (2001).

Recently, Kuhlbrodt et al. (2006) analysed the different sources of energy for driving the MOC from the knowledge obtained from existing modeling as well as measurement studies. They concluded that even though the surface buoyancy forcing is not considered as a driver of the MOC capable of providing energy supply, it is nevertheless necessary for setting up the flow by controlling the rate and site of deep water formation.

In summary, the previous studies considered three candidates capable of driving and/or affecting the MOC : the diapycnal mixing, the wind-driven upwelling and the *mean* buoyancy forcing at the sea surface. A fourth candidate, namely the day-to-day *anomalies* of air-sea fluxes, is studied in this thesis through a modeling approach. The focus is on the identification and understanding of the effects of the flux anomalies. The primary research question is :

Whether and how do daily flux anomalies affect the strength of the MOC ?

There are reasons to believe that the fluctuating daily fluxes can, at least in principle, play a role in determining the strength of the global MOC. Firstly, fluctuations in winds can generate turbulent motions, thereby inducing additional mixing. Secondly, fluctuations in the buoyancy forcing can alter the stability and trigger or hamper convective events, leading to changes in the mixing structure not only near the surface but also in the deep ocean. More importantly, the effect of fluctuating fluxes can highly be non-linear. For instance, while a positive buoyancy flux anomaly does not produce additional convective events in a mostly stable region, a negative one can reduce the stability and lead to changes in the convective mixing. Due to such non-linearity, fluctuating fluxes, though not contributing to the total flux forcing on the time average, are capable of modifying the turbulent mixing on global scales and from that the global MOC. It will be shown in this thesis that the flux anomalies have an impact on global time-mean circulation and affect not only the Atlantic MOC, but also the ACC by changing the vertical mixing in the model ocean.

The processes related to diapycnal mixing cannot explicitly be resolved by a coarse resolution ocean GCM (O-GCM). Measurements of vertical mixing in the real ocean suggest that the mixing is vertically and spatially non-uniform. Smaller values of the order of 10^{-5} $m^2 s^{-1}$ are measured away from topography (Ledwell et al., 1993) and close to the equator (Gregg et al., 2003). Higher values of up to 10^{-3} $m^2 s^{-1}$ are observed along continental slopes (Moum et al., 2002) and rough topography (Polzin et al., 1997; Ledwell et al., 2000). Mixing values ranging from 10^{-6} to 10^{-3} $m^2 s^{-1}$ over under-sea topographic features in the southern subtropical Atlantic, Indian and Pacific sectors of the Southern ocean are estimated by Sloyan (2005). The mixing reported by these authors results presumably from the breaking of internal waves within the ocean. The present study employs another type of vertical mixing which results from daily surface fluxes and can also vary both geographically and vertically, depending on the surface fluxes.

The effects of air-sea flux anomalies can hardly be separated from the effect of the climatological mean flux within a fully coupled atmosphere-ocean GCM (AO-GCM). For this reason, an empirical model of flux anomalies is used. Numerical experiments performed by an O-GCM driven by climatological mean air-sea fluxes plus various types of flux anomalies are carried out. The experiments are designed such that they allow an identification and quantification of the effects of the flux anomalies.

The thesis is structured as follows: The simple atmospheric model used for this study is introduced in chapter 2. The coupled model and the numerical experiments are described in chapter 3. The results of the experiments and discussion of the separate roles of the *feedback* and *fluctuation* parts of the daily flux anomalies are presented in chapter 4. Conclusions are given in the final chapter 5.

2. AN ANOMALY MODEL FOR AIR-SEA FLUXES : EMAD

In this chapter, the simple atmospheric model, that is used in this study is introduced. Since the model is empirical and captures the linear dynamics of air-sea interaction, it will be referred to as EMAD (Empirical Model of Atmospheric Dynamics) (von Storch et al., 2005). The first section gives an overview of some examples of previous simple models of surface fluxes. A detailed description of EMAD and the estimation procedure of the model parameters are given in sections 2.3 and 2.4, respectively. To analyze the performance of EMAD, the response of EMAD to different anomalous sea surface conditions is studied in section 2.4.1. Since EMAD is designed to describe the statistics, rather than to predict individual fluxes for a given sea surface condition, section 2.4.2 concentrates on the ability of EMAD to produce realistic flux statistics, namely, a) the total variances and b) the cross-correlation functions between fluxes and the SST, which represent different types of air-sea interactions. For this purpose, uncoupled EMAD integrations and an integration of EMAD coupled to the HOPE-G ocean GCM are considered. It will be shown that the important types of air-sea interactions identified in the coupled AO-GCM are, by and large, captured by the EMAD model. This chapter is concluded in section 2.5.

2.1 Different simple flux models

An O-GCM is driven by fluxes of momentum, heat and freshwater at the sea surface. An advanced approach is to represent the fluxes with the aid of parameterisations implemented in an atmospheric GCM (A-GCM). A simpler approach is to prescribe the fluxes in the form of simple atmospheric models. Generally, a simple approach is often based on certain assumptions and is designed to represent part of the fluxes which are needed for studying a particular phenomenon (e.g., the thermohaline circulation (THC), El-Niño and southern oscillation (ENSO)). The following gives an introduction to different simple models of flux anomalies. Hereafter, the fluxes of heat, freshwater and momentum are denoted by H, F and M respectively. They can be decomposed into climatological mean annual cycles, H_c, F_c and M_c, and deviations from the climatological annual cycles, $H^{'}$, $F^{'}$ and $M^{'}$.

a) Traditional mixed boundary condition for studying the thermohaline circulation

The traditional mixed boundary condition (Haney, 1971) focuses on the formulation of heat and freshwater fluxes. It is used to study the thermohaline circulation of the ocean. It can be written as

$$H_t = \alpha(T^* - T_t) = H_c - \alpha T_t^{'}, \qquad F_t = F_c, \qquad M_t = 0. \tag{2.1}$$

The heat flux H_t is obtained by restoring SST T_t, to a prescribed temperature T^* with a restoring coefficient α. $1/\alpha$ gives the restoring time. When decomposing T_t into its climatological mean annual cycle T_c and the deviation from T_c, $T^{'}$, H_t can be decomposed into a climatological flux $H_c = \alpha(T^* - T_c)$ plus a flux anomaly $H^{'} = -\alpha T_t^{'}$. The latter assumes that any deviation of oceanic temperature from the climatological mean value will lead to a heat flux which acts to damp out the deviation. The damping occurs as soon as there is a deviation, implying that the atmosphere adjusts to changes in the ocean quickly as if it is in a quasi-equilibrium state with the ocean. The restoring time scale, $1/\alpha$ is often of the order of a month, so that the ocean temperature anomalies can only freely evolve within the time scales of about a month.

The freshwater flux can also be described in a form similar to that of H_t, i.e. $F_t = F_c - \alpha S_t^{'}$, where $S_t^{'}$ is the salinity anomaly. However, in contrary to SST anomalies which can be damped out by the heat flux anomalies, the freshwater flux anomalies are not directly related to the salinity anomalies at the sea surface. Thus, salinity anomalies stay in the ocean for much longer time than SST anomalies. One can assume the limit of infinite restoring time, i.e. α can be taken as zero. The freshwater flux can then be represented by a constant flux F_c.

The traditional mixed boundary condition considers the variations in heat flux originating only from the ocean and prescribes the freshwater flux.

b) Improved mixed boundary condition

The above traditional mixed boundary condition oversimplifies the interaction between SST and heat flux. It implies that temperature anomalies on all scales will be damped out at the same rate, which is determined by α. By using a single, constant restoration time, both large-scale and small-scale temperature anomalies that have developed anywhere in the ocean will be damped in the same way. In a more realistic case, large-scale SST anomalies are damped out more slowly than small-scale anomalies. In order to take this into account, a scale-dependent restoration was suggested by Willebrand (1993) and Rahmstorf and Willebrand (1995). They introduced an improved mixed boundary condition by considering a scale-dependent representation of the heat flux, derived from a simplified, atmospheric energy balance model (EBM).

The different components of the total heat flux, namely, sensible and latent heat, net shortwave and longwave radiations, and horizontal heat transport of the atmosphere are linearised in terms of air/sea temperatures. As a result, the heat flux at the sea surface is described by two processes of the EBM. One represents the temperature relaxation due to the emission of excess heat from the top of the atmosphere to the outer space to compensate the increased heat flux from the ocean. This contribution to H_t is given by $\gamma(T^* - T_t)$. The other process is the lateral diffusion of heat due to atmospheric eddy transport, given as $\mu\nabla^2(T^* - T_t)$. The relaxation constant γ is generally smaller than μ. The improved formulation takes the form

$$H_t = \gamma(T^* - T_t) - \mu\nabla^2(T^* - T_t), \qquad F_t = F_c, \qquad M_t = 0, \tag{2.2}$$

where T^* is the temperature towards which the ocean is forced. The operator ∇^2 is strongly scale-selective. For small-scale temperature anomalies, the magnitude of the diffusive term is large and for large-scale temperature anomalies, the magnitude of the diffusive term is small. Hence, small-scale anomalies are damped quickly and large-scale anomalies are allowed to exist over a long time. The freshwater flux forcing F_t is independent of the oceanic changes. Its formulation is unchanged.

This improved mixed boundary condition was successfully tested in studies of large-scale changes in the THC using an ocean-only model (Rahmstorf and Willebrand, 1995). They suggest to estimate the relaxation coefficients, γ and μ either from observations or from model data. The present study further generalises the representation of heat flux by using data from a coupled AO-GCM (see section 2.3).

c) Empirical model for ENSO study

Another example of a simple flux model focuses on momentum fluxes and is used to study the oceanic aspects of the ENSO mechanisms (Latif and Villwock, 1990). This empirical model reads

$$H_t = 0, \qquad F_t = 0, \qquad M_t = M_c + \nu \, T_t^{'}, \tag{2.3}$$

where ν is a set of regression coefficients estimated from the SST data of an ocean model forced by observed winds. The expression $M_t = M_c + \nu \, T_t^{'}$ in Eq.(2.3) relies on the assumption that the wind stress, after being perturbed by an SST anomaly, can quickly reach a quasi-stationary state with this SST anomaly. Hence, the fluxes can be considered as quasi-stationary responses to the SST anomaly. In Eq.(2.1), where α is always negative, SST anomalies are always damped by heat flux anomalies. Whereas in Eq.(2.3), ν can be positive too i.e. positive SST anomalies can lead to westerly wind anomalies in the tropical Pacific during the warm event of ENSO. Despite its simple form of linear and local SST-wind stress interaction, this model is able to simulate a significant part of the interannual variability of the tropical Pacific ocean.

d) Purely stochastic forcing for studying low-frequency variability

A further formulation focuses on the freshwater flux (Mikolajewicz and Maier-Reimer, 1990). Since $P - E$ (precipitation$-$evaporation) is not a function of SST, the freshwater flux is considered as a purely stochastic forcing of the atmosphere. This simple model is used to study the oceanic variability on time scales of a few centuries. It takes the form,

$$H_t = \alpha(T^* - T_t) = H_c - \alpha T_t^{'}, \qquad F_t = F_c + F_t^{'}, \qquad M_t = M_c, \tag{2.4}$$

where $F_t^{'}$ is a spatially correlated white-noise freshwater flux. This stochastic forcing in freshwater flux excited low-frequency internal oceanic variability. The results obtained with this formulation show that random atmospheric fluxes can excite long-term variability in the ocean.

e) Shortcomings of previously used simple flux models

- In general, each of the simple models captures only a specific type of air-sea processes and is used to study a specific aspect of the coupled system. The traditional and improved mixed boundary condition (Eq.(2.1) and Eq.(2.2)) concentrate on the bouyancy forcing and are used to study the thermohaline circulation. The empirical wind stress model (Eq.(2.3)) assumes a linear relation between anomalies of the wind stress and SST and is used to study ENSO in the tropical Pacific ocean. The purely stochastic freshwater forcing (Eq.(2.4)) considered the atmosphere as a noise generator for the ocean to study oceanic low-frequency variability. None of the models are designed to take all possible air-sea interactions into account.

- Apart from the stochastic freshwater forcing in Eq.(2.4), the variations in heat fluxes produced by Eq.(2.1) and Eq.(2.2) and those in momentum fluxes produced by Eq.(2.3) originate solely from the ocean. In reality, both heat flux and freshwater flux vary strongly due to atmospheric turbulence. A realistic flux model should take such variations into account.

- None of the previous models considered regions where sea-ice can be formed. Consequently, they cannot be used to drive a global ocean model including sea-ice.

2.2 A measure of different types of air-sea processes

For the present study, a flux model which is able to reproduce all air-sea processes present in a fully coupled AO-GCM is needed. To ensure that EMAD is able to do the job, a simple measure of different air-sea processes is desirable. Previous studies (Frankignoul 1985, 1990; von Storch, 2000) demonstrated that the cross-correlation functions can be used as such a measure.

Consider the cross-covariance function, $R_{xy}(\tau)$ between an atmospheric flux x at a certain grid point and an oceanic variable y (e.g. SST) at the same grid point

$$R_{xy}(\tau) = \overline{x_t^{'} y_{t+\tau}^{'}} \tag{2.5}$$

Here $\bar{}$ indicates the time average, τ indicates the time lag and $x^{'}$ and $y^{'}$ denote deviations from the corresponding climatological mean annual cycles. R_{xy} is generally not symmetric about $\tau = 0$. This feature can be used to distinguish the situation when atmosphere x leads (i.e. $\tau > 0$) from the situation when ocean y leads (i.e. $\tau < 0$). Different air-sea interactions are characterized by different shapes of the cross-covariance functions. Figure 2.1 shows covariance functions related to three types of air-sea interactions.

The cross-covariance function indicated by the thin solid line in Figure 2.1 is obtained when $x^{'}$ responds to $y^{'}$ occurring at an earlier time $t-\Delta$ such that $x_t^{'} = const \times y_{t-\Delta}^{'}$. Multiplying this relation by $y_{t+\tau}^{'}$ and applying the average operator $\bar{}$ on the result, one finds $R_{xy}(\tau) = const \times R_{yy}(\tau + \Delta)$ where R_{yy} is the auto-covariance function of the oceanic variable. R_{xy} peaks at time lag $-\Delta$ when y leads and is symmetric about $-\Delta$. When $\Delta = 0$ is assumed, as for H in Eq.(2.1) and for M in Eq.(2.3), $R_{xy}(\tau)$ would be symmetric about $\tau = 0$. If the heat flux and momentum flux can indeed be

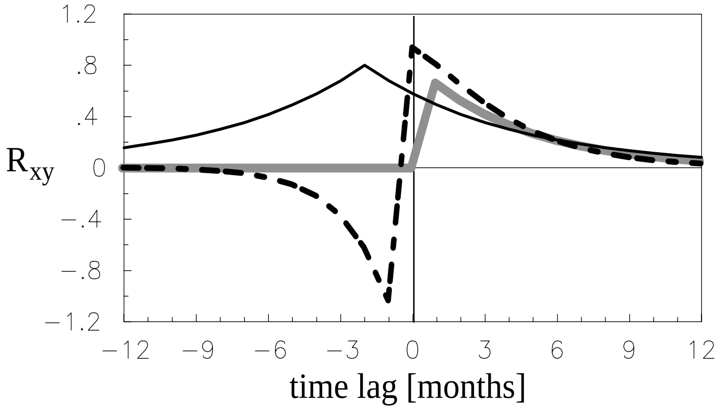

Fig. 2.1: Cross covariance functions characterizing three idealized types of air-sea interactions. Positive (negative) time lags in months correspond to the situation when atmosphere leads (ocean leads).

described as a quasi-stationary response to SST as in Eq.(2.1) and Eq.(2.3), the cross-correlation functions between H and SST and between M and SST would be similar to the thin solid line. As will be shown in section 2.4.2b, this is not true in general.

The thick gray line in Figure 2.1, on the other hand, describes the situation when $y^{'}$ is generated by $x^{'}$, and after being generated, $y^{'}$ does not feedback to $x^{'}$. In this case, R_{xy} peaks when $x^{'}$ leads and is zero when $y^{'}$ leads. The detailed shape of R_{xy} for $\tau > 0$ depends on the memory of $x^{'}$ and $y^{'}$. This type of cross-covariance function describes the relation between the freshwater flux and the SST in Eq.(2.4). If the atmospheric flux is a stochastic forcing of the ocean, one would obtain a cross-covariance function between the flux and SST which is of the type indicated by the gray line. As will be shown later, such cross-covariance functions are found for wind stress and SST in the mid- and high-latitude regions in a coupled GCM.

Finally, the dashed line in Figure 2.1 describes the situation when $y^{'}$ is first generated and then damped by $x^{'}$, which leads to an anti-symmetric

R_{xy} (Frankignoul, 1985). If the mixed boundary condition (section 2.1a and b) is appropriate, one would not obtain this anti-symmetric shape. But section 2.4.2b shows the opposite. The relation between heat flux and SST are described by an anti-symmetric cross-covariance function in most extra-tropical regions. Such relations are found in observations (Frankignoul et al., 1998) and in an integration with the coupled ECHAM3/LSG AO-GCM (von Storch, 2000).

Cross-correlation functions will be used later to validate the air-sea processes produced by EMAD in section 2.4.2b.

2.3 Description of EMAD

The following section introduces a new simple atmospheric model, EMAD, which is able to capture different types of air-sea interactions. The main difference between EMAD and the previous simple models is that the model is not built on one particular assumption, but is described by a general form which allows different types of interactions, depending on the model parameters. The model is empirical, since the model parameters are obtained by fitting the model to an integration with a coupled AO-GCM. It consists of a deterministic part and a noise part. The former describes the linear dynamics of the fluxes and the linear responses of fluxes to sea surface conditions. The model aims to reproduce the variances found in an A-GCM and furthermore, when coupled to an O-GCM, to reproduce the same types of cross-covariance functions as found in the coupled AO-GCM. It can be considered as statistically equivalent to an A-GCM with respect to second moments of the time-varying surface fluxes.

EMAD is formulated for deviations from the climatological mean annual cycle. It is assumed that the deviations are small. The smallness ensures the validity of the linear equation,

$$\mathbf{x}'_{t+1} = \mathcal{A}\mathbf{x}'_t + \mathcal{B}\mathbf{y}'_t + \mathcal{C}\mathbf{n}_{t+1}. \tag{2.6}$$

(Hereafter, bold letters indicate vectors and bold capital italics indicate matrices). $\mathbf{x}'$ consists of all fluxes required to drive an O-GCM. $\mathbf{y}'$ represents the oceanic variables at the sea surface that can affect $\mathbf{x}'$, such as the SST and the sea-ice cover. The matrix $\mathcal{A}$ depicts the linear behavior of the fluxes, $\mathcal{B}$ the linear responses of the fluxes to oceanic anomalies at the sea surface, and $\mathcal{C}$ the covariance structure of the part of $\mathbf{x}'$ that is not captured by $\mathcal{A}$ and $\mathcal{B}$. $\mathbf{n}$ is a multivariate white noise with zero mean and unit variance. The stochastic forcing $\mathcal{C}\mathbf{n}$ is white in time, but not in space.

Equation (2.6) suggests that EMAD is able to describe different types of air-sea interactions. If the second term on the right hand side of Eq.(2.6) dominates, EMAD would only produce linear responses of $\mathbf{x}'$ to $\mathbf{y}'$, just as Eq.(2.1) and Eq.(2.3). On the other hand, if the second term is negligible, the variations in the fluxes would be generated by the atmosphere. These fluxes would appear as stochastic forcing and can generate variations in $\mathbf{y}'$. Once being generated, $\mathbf{y}'$ would not feedback to $\mathbf{x}'$. Cross-covariance functions resembling the gray line in Figure 2.1 would be observed. Finally, if the three terms on the right hand side of Eq.(2.6) are of comparable strength, $\mathbf{y}'$ would be generated via both the stochastic forcing and the feedback from the ocean. The cross-covariance function related to this type of air-sea interactions would be described by the dashed line in Figure 2.1. Generally, the relative importance of the three terms varies geographically and depends on which flux is considered.

Since $\mathcal{B}$ in the second term is derived from a coupled model integration which is essentially statistically stationary, the interaction described by $\mathcal{B}\mathbf{y}'$ acts to keep the ocean in the given mean state . This means that if the ocean is moved away from the mean state, there would be non-zero anomalies of oceanic variables and from that a non-zero $\mathbf{y}'$, which generates anomalous fluxes $\mathcal{B}\mathbf{y}'$ that drive the ocean back to the given mean state.

It will be shown in chapter 4 that the above discussed oceanic feedback involves essentially the interaction between the heat flux and the SST anomalies . It functions in a way as if the heat flux was described by the restoring condition in section 2.1a. However, different from the traditional restoring formulation, which uses a constant restoration time, $\mathcal{B}$ implies a scale-dependent restoration time. By being formulated in EOF-space, $\mathcal{B}$ captures the restoring time scales for modes with different spatial scales in the integration of the AO-GCM ECHO-G (see Appendix). In particular, large-scale SST anomalies are allowed to exist over longer time periods, while small-scale SST anomalies will be damped out quickly as suggested by Rahmstorf and Willebrand (1995). The present formulation can be considered as an empirical approach that captures the scale-dependent feedback between SST and heat flux by fitting Eq.(2.6) into the ECHO-G integration.

By collecting all fluxes into vector $\mathbf{x}$ and all relevant sea surface variables into vector $\mathbf{y}$, the model equation (2.6) ensures that the fluxes and oceanic variables are physically coherent. When coupling EMAD to an O-GCM, the fluxes of heat, freshwater and momentum cannot act independently to given anomalous sea-surface conditions.

Eq.(2.6) represents only the general form of EMAD. In practice, the model has a much more complicated structure. It operates in two spaces and has two modules.

2.3.1 Two spaces of EMAD

The number of grid points in the ECHO-G model is 3056. Hence, the dimensions of each flux of $\mathbf{x}'$ and each oceanic variable of $\mathbf{y}'$ are easily of the order of 10^4. In order to avoid overfitting and furthermore to simplify the estimation procedure, the data are first compressed. This leads to the usage of a reduced EOF-space and the full grid-point space. $\mathcal{A}$ and $\mathcal{B}$ are estimated in the reduced space spanned by the leading EOFs. The fluxes produced by the deterministic part of EMAD, $\mathcal{A}\mathbf{x}_t^{'} + \mathcal{B}\mathbf{y}_t^{'}$, are then transformed back to the grid-point space, where the stochastic forcing $\mathcal{C}\mathbf{n}$ is added. $\mathcal{C}$, which represents the covariance structure of the errors which are not described by $\mathcal{A}$ and $\mathcal{B}$, has much smaller spatial scales than fluxes produced by the deterministic part of EMAD. This matrix is obtained in the grid-point space and separately for each flux. The final outputs of EMAD are fluxes at all grid points.

Note that the general EMAD ansatz (2.6) allows for non-local relationships between fluxes and oceanic variables at different grid points. The noise term acts to excite the EOF-modes described by the deterministic part of EMAD (i.e. by $\mathcal{A}$- and $\mathcal{B}$-terms). The matrix $\mathcal{C}$ also ensures that the distributions of the total variances of the fluxes match those obtained from the coupled ECHO-G into which EMAD is fitted.

The EOFs are calculated for the daily time series for each flux in $\mathbf{x}^{'}$ and for each variable in $\mathbf{y}^{'}$. For the EMAD version used here, the number of EOFs chosen for each flux in $\mathbf{x}^{'}$ and for each oceanic variable in $\mathbf{y}^{'}$ is 100 in the water module and 50 in the ice module. The modules are defined below. Each included EOF explains at least 0.25% of the total variance of the respective variable. The cumulative variance explained by these EOFs ranges from 50 to 80%, depending on the flux considered. Note that since daily data are used, the leading EOFs for fluxes represent synoptic-scale variations and explain only a few percentages of the respective total variances.

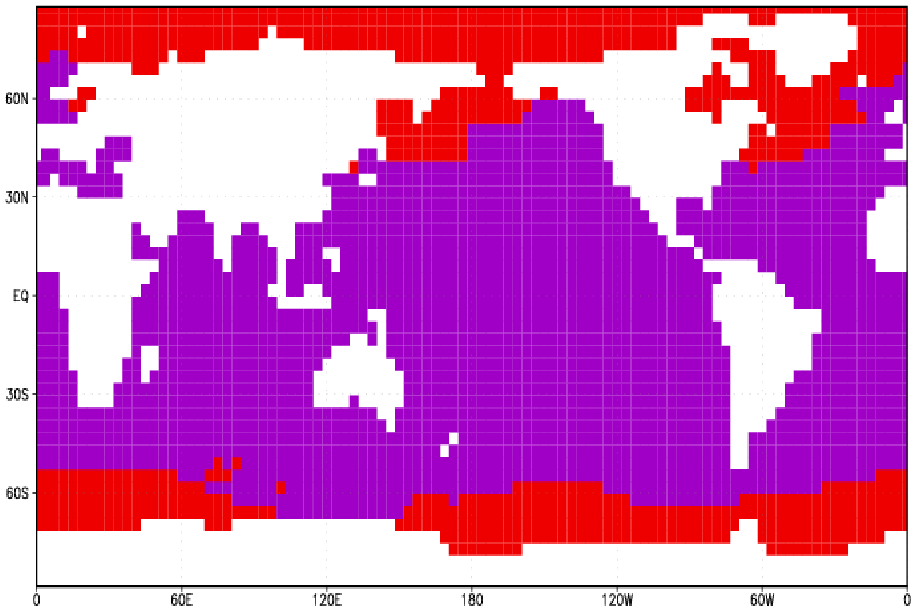

Fig. 2.2: The domains of the two modules of EMAD model in T30 resolution. The region of the water-module is shaded in indigo and the region of ice-module is shaded in red.

2.3.2 Two modules of EMAD

The air-sea coupling in ice-free regions differs from that in regions where sea-ice can be formed. As a consequence, the surface fluxes as well as the oceanic conditions that affect the fluxes are different in the two regions. To describe these different coupling processes, two modules are used. The water-module is defined in regions where sea-ice cannot be found all year round and the ice-module is defined in regions where the formation of sea-ice is permitted. The boundary is derived from the ECHO-G-integration and fixed afterwards. The domains of the two modules are shown in Figure 2.2. For each of the two modules, a set of matrices $\mathcal{A}$, $\mathcal{B}$ and $\mathcal{C}$ is derived.

The main difference between the two modules is that the ice-module contains much more fluxes than the water module. First of all, one has to consider the residual and conductive heat flux required to describe the formation or melting of the ice. In addition to that, since a grid cell in the domain of the ice-module contains an ice-covered and an ice-free part where different dynamics take place, fluxes over ice-covered and ice-free part of a grid cell have to be treated separately. In general, $\mathbf{x}$ in a grid cell in the domain of the ice module consists of $\mathbf{x}^{free}$ and $\mathbf{x}^{ice}$. The former enters the ocean beneath the ice-free part of the cell, whereas the latter interacts with the sea-ice. The net flux in a grid cell is

$$\mathbf{x}_t = \mathrm{A}_t \mathbf{x}_t^{ice} + (1 - \mathrm{A}_t)\mathbf{x}_t^{free}, \tag{2.7}$$

where A_t is the fractional sea-ice cover produced by the ocean model which contains a sea-ice model.

2.3.3 Estimation of matrices $\mathcal{A}$, $\mathcal{B}$ and $\mathcal{C}$

200 years of daily data obtained from an ECHO-G integration (see Appendix) are used for the derivation of the model parameters. Such a long integration is necessary to obtain reliable estimates of $\mathcal{A}$, $\mathcal{B}$ and $\mathcal{C}$. Since EMAD is an anomaly model, only deviations from the climatological mean annual cycle with the period of 360 days are used. Being derived from daily data, the time step of EMAD is one day.

The matrices $\mathcal{A}$ and $\mathcal{B}$ are derived in the EOF-space. For this purpose, each flux in $\mathbf{x}$ and each sea surface variable in $\mathbf{y}$ are projected into their corresponding EOF-space. $\mathbf{p}_{x,t}$ and $\mathbf{p}_{y,t}$ compose the principle components of all fluxes contained in $\mathbf{x}$ and all sea-surface variables contained in $\mathbf{y}$ at t, respectively. The one-time-step prediction by EMAD in the EOF-space reads

$$\hat{\mathbf{p}}_{x,t+1} = \mathcal{A}\mathbf{p}_{x,t} + \mathcal{B}\mathbf{p}_{y,t}.$$

where $\hat{\mathbf{p}}$ indicates the principle components predicted by the deterministic part of the EMAD. The matrices $\mathcal{A}$ and $\mathcal{B}$ are obtained by minimizing the mean squared differences between $\hat{\mathbf{p}}_{x,t}$ and the true principle components $\mathbf{p}_{x,t}$, as obtained from the integration with the ECHO-G,

$$< (\mathbf{p}_{x,t} - \hat{\mathbf{p}}_{x,t})^2 >= min.$$

As the solution of the minimization, one obtains

$$\mathcal{A} = ({\Sigma_1}^T - {\mathcal{C}_1}^T\Pi^{-1}\mathcal{C}_0)({\Sigma_0}^T - {\mathcal{C}_0}^T\Pi^{-1}\mathcal{C}_0)^{-1},$$

$$\mathcal{B} = ({\mathcal{C}_1}^T - \mathcal{A}{\mathcal{C}_0}^T)\Pi^{-1}$$

where ^{T} denotes transpose and $^{-1}$ denotes inverse. Σ_1 is the lag-1 covariance matrix, Σ_0 the lag-0 covariance matrix of $\mathbf{p}_x$ and Π is the lag-0 covariance matrix of $\mathbf{p}_y$. As principal components are used for the minimization, Σ_0 and Π are diagonal. $\mathcal{C}_0$ denotes the lag-0 cross-covariance matrix between $\mathbf{p}_x$ and $\mathbf{p}_y$, $\mathcal{C}_1$ the cross-covariance matrix at lag one day.

Having obtained $\mathcal{A}$ and $\mathcal{B}$, $\mathcal{A}\mathbf{p}_{x,t} + \mathcal{B}\mathbf{p}_{y,t}$ can be transformed into the grid point space for each t. The resulting time series for a flux is denoted by $\hat{\mathbf{x}}_t$. The residual of this flux which is not described by the deterministic part of the EMAD is

$$\mathbf{x}_t - \hat{\mathbf{x}}_t = \zeta_t.$$

The matrix $\mathcal{C}$ is determined such that $\mathcal{C}\mathbf{n}$ describes the covariances of the residual time series ζ_t, with $\mathbf{n} = (n_1, \cdots, n_m)^{-1}$ being a zero-mean multivariate white noise. This is the case when

$$\mathcal{C} = (\mathbf{e}_1, \mathbf{e}_2, ...\mathbf{e}_m),$$

where $\mathbf{e}_i$ with $i = 1, \cdots, m$ are EOFs of ζ_t, and the variance of the i-th component of $\mathbf{n}$ equals the eigenvalue λ_i that corresponds to eigenvector $\mathbf{e}_i$. In this case, the covariance matrix of $\mathcal{C}\mathbf{n}$ equals the covariance matrix of ζ.

a) **EMAD**

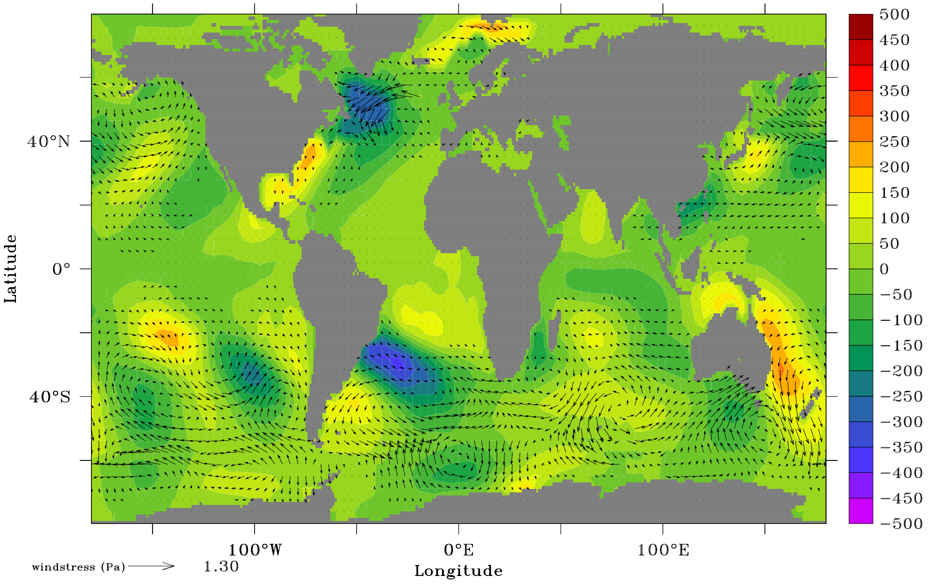

Heat Flux Anomaly (W/m^2), EMAD

b) **NCEP**

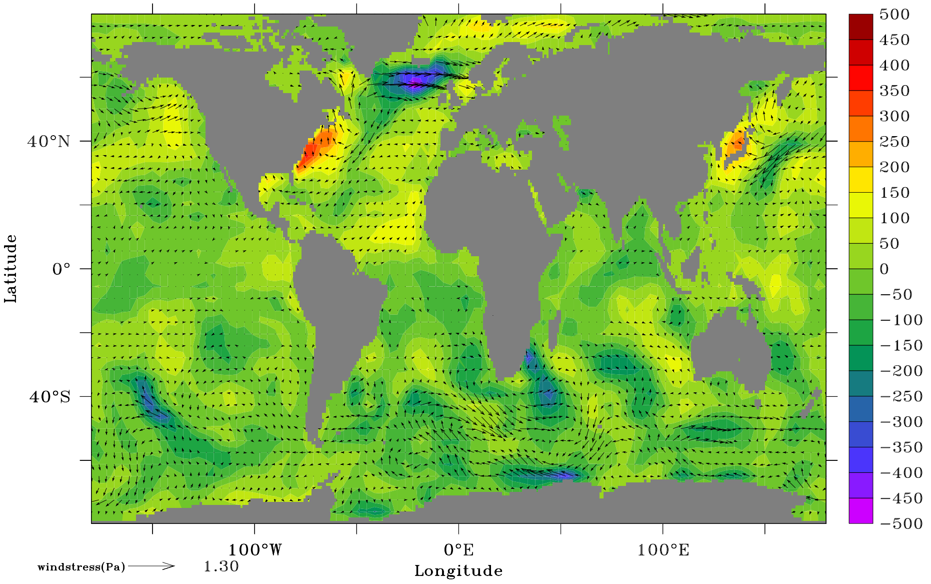

Heat Flux Anomaly (W/m^2), NCEP

Fig. 2.3: Daily snapshots of wind stress and heat flux anomalies from a) EMAD model and b) NCEP/NCAR Reanalysis. The units are in *Pascal* and W/m^2 respectively.

2.4 Validation of EMAD

To give the reader an idea of fluxes generated by EMAD, Figure 2.3 shows anomalies of wind stress (arrows) and heat flux (colour shading) as obtained by forcing EMAD with the anomalous sea-surface conditions derived from the coupled ECHAM5/MPI-OM AO-GCM (see Appendix). Also shown in Figure 2.3 is a snapshot of the anomalies of the same fluxes from the NCEP reanalysis for an arbitrary day. Similar to the fluxes of the reanalysis, the EMAD-fluxes have maxima at the mid- and high-latitudes. The amplitudes of EMAD-anomalies are slightly larger than those of the reanalysis. The structure of the EMAD-anomalies is somewhat smoother than that of the NCEP-fluxes, reflecting the fact that EMAD describes the leading EOF-modes excited by a white noise forcing.

2.4.1 Stationary responses to different oceanic conditions

To test how EMAD reacts to different oceanic forcing, stationary responses to two idealized oceanic conditions are considered. The response patterns are given by

$$\mathbf{x} = (\mathcal{I} - \mathcal{A})^{-1} \, \mathcal{B}\mathbf{y} \tag{2.8}$$

where $\mathbf{y}$ represents the oceanic condition and $\mathcal{I}$ is the identity matrix. Eq.(2.8) is obtained using the stationarity condition: $\mathbf{x}_{t+1} = \mathbf{x}_t$. One can also derive the response numerically by integrating EMAD for a given constant $\mathbf{y}$. In this case, the solution will approach Eq.(2.8) after some integration time. The response patterns discussed below are derived for a given $\mathbf{y}$ according to Eq.(2.8).

a) Stationary responses to El-Niño-related SST anomalies

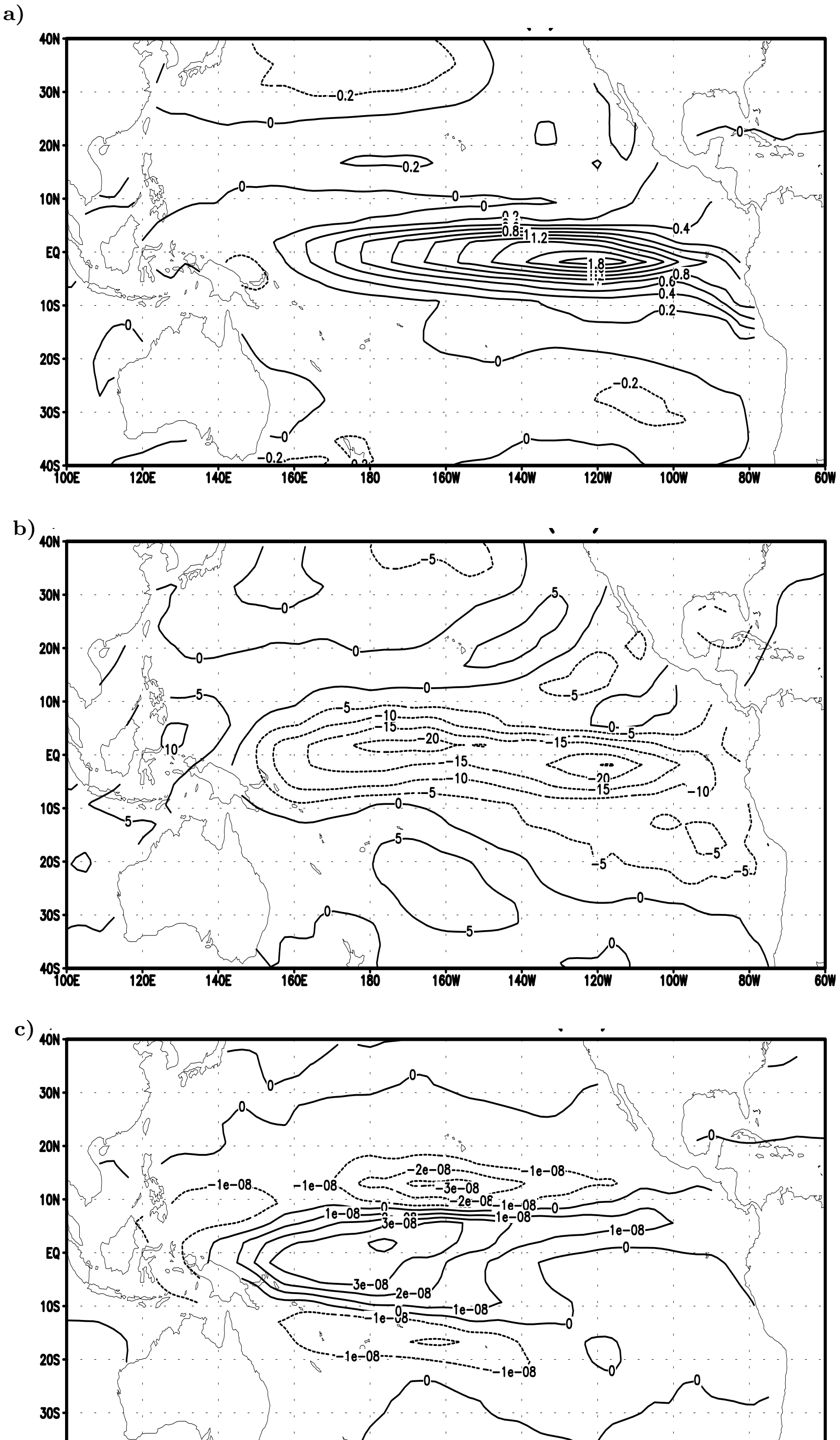

Fig. 2.4: Stationary responses of EMAD to a) El Nino SST anomalies (^{o} C) in terms of b) net heat flux (W/m^2) and c) net freshwater flux (m/s).

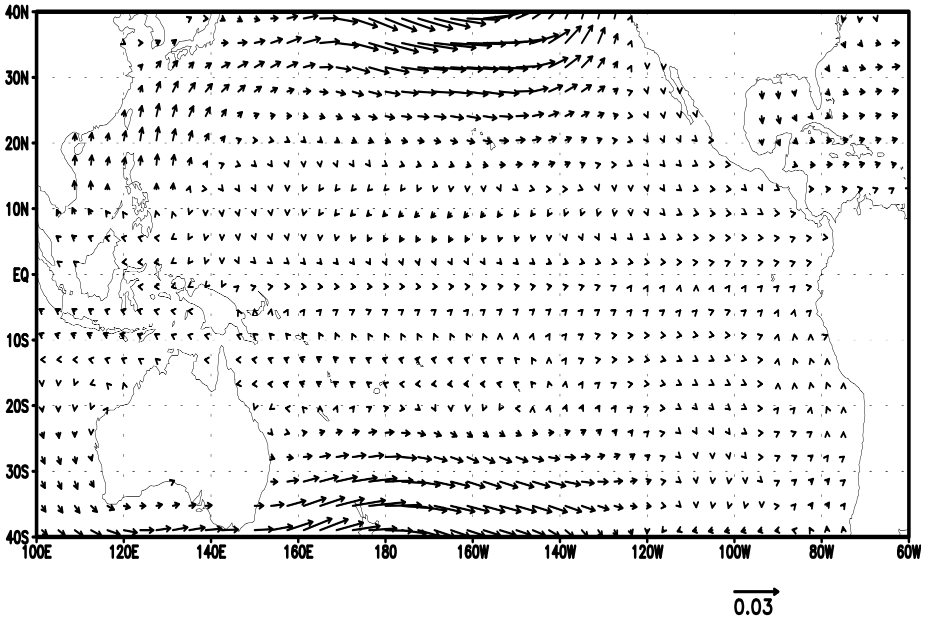

Fig. 2.5: Stationary responses of EMAD to El Nino SST anomalies in terms of momentum flux anomalies (Pa).

The first oceanic condition considered here is the first EOF of the Pacific SST in the ECHO-G integration which describes typical ENSO-related SST-anomalies in the tropical Pacific produced by the ECHO-G model. The maximum SST anomaly reaches 1.8^{o}C in the eastern equatorial Pacific near 120^{o}W (Figure 2.4a).

Figure 2.4b and c show EMAD's responses in the net heat and fresh water flux to the El-Nino SST anomalies. The heat flux anomalies are negative (upward) and characterized by two maxima located in the central and eastern tropical Pacific (near 165^{o}W and 120^{o}W) respectively. The structure of the heat flux anomalies in the eastern Pacific suggests that these anomalies represent upward sensible heat fluxes induced by warmer than normal SST in that region. The maximum in the central Pacific on the other hand results not only from changes in sensible heat flux, but also from changes in short wave radiation (not shown). As indicated by Figure 2.4c, EMAD produces stronger than normal precipitation in response to the

SST anomalies. These precipitation anomalies lead to a reduction in the downward short wave radiation, reflecting an increase in cloudiness which contributes to the negative maxima of the net heat flux in the central Pacific.

The wind stress response pattern (Figure 2.5) reveals westerly wind-stress anomalies throughout the equatorial Pacific. Large wind stress anomalies in the North Pacific are consistent with the pattern of Pacific North America (PNA) circulation, which is observed to be related to the SST anomalies in the tropical Pacific.

The stationary responses are comparable with anomalies observed during an El Niño event. For instance, Figure 2.4b strongly resembles the distribution of heat flux anomalies found during the 1986-87 El Niño (Sun 2003). Figure 2.4c is consistent with strong negative values of outgoing long wave radiation observed during 1982-83 El Niño (Philander,1990), which indicate enhanced precipitation and thus positive freshwater flux anomalies over the central tropical Pacific.

The example of EMAD's response to El Niño-related SST anomalies demonstrates that EMAD is able to produce responses to SST-changes with respect to all fluxes needed by an ocean model, rather than to just one particular flux. This marks one of the major differences between EMAD and the other simple models of fluxes that were described in section 2.1.

b) Stationary responses to a polynya

The second anomalous oceanic condition is a big "polynya" in the Arctic. The size of the polynya is about 25^o longitude by 8^o latitude, indicated by the box in Figure 2.6b. It is placed just to the northern border that separates the domains of the water and ice modules. Within the polynya, SST is set to 0^oC and the sea-ice cover A to zero.

EMAD responds to the polynya condition by producing an anomalous

a) net heat flux and wind stress anomalies

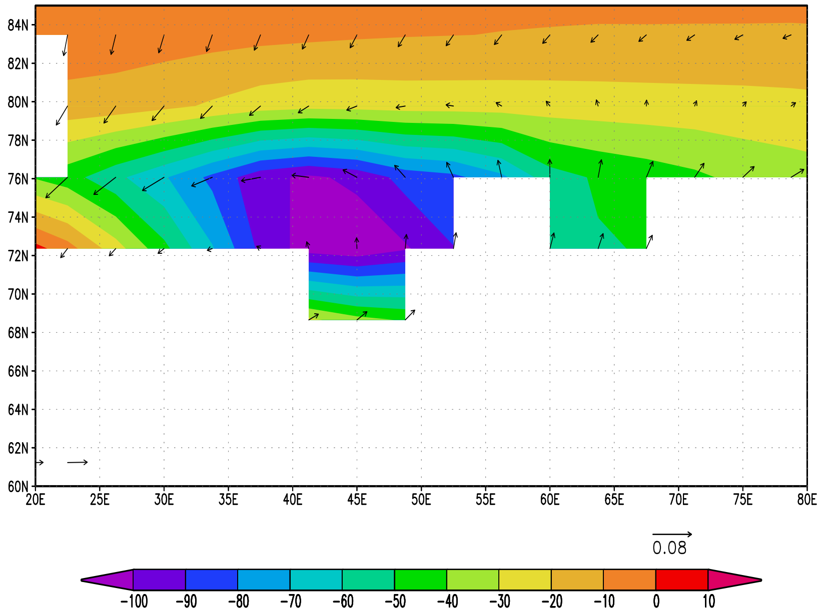

b) freshwater flux anomalies

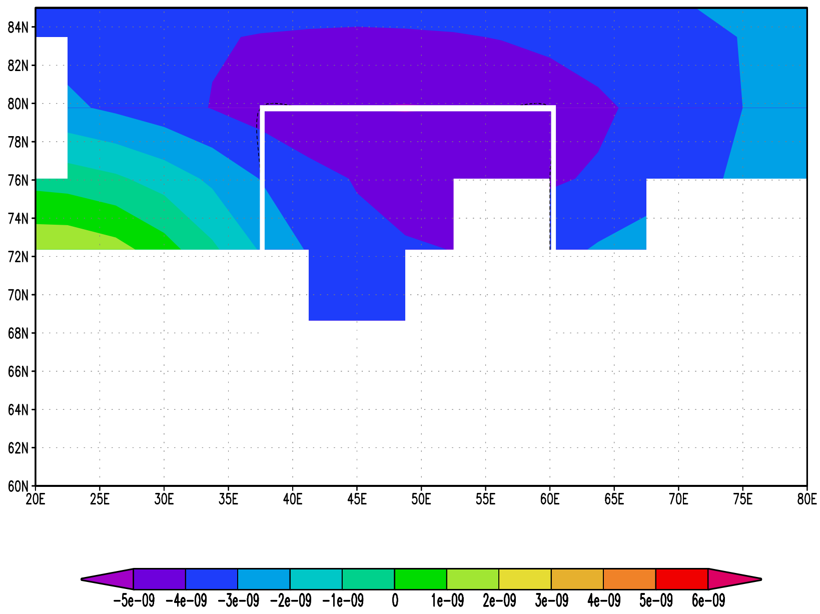

Fig. 2.6: Stationary responses of EMAD in the region (20E-80E, 60N-84N) to a polynya in terms of a)net heat flux (W/m^2) and wind stress (Pa) and b)freshwater flux. The polynya is marked by the box in b) and the land surface is shaded in white.

upward (negative) net heat flux of up to 100 W/m^2 (shading in Figure 2.6a). This heat source leads to an anomalous cyclonic circulation associated with anti-clockwise wind stress anomalies (arrows in Figure 2.6a). Furthermore, it also causes stronger than normal evaporation and from that an anomalous upward (negative) fresh water flux (Figure 2.6b). The cyclonic anomalies and net heat loss shown in Figure 2.6 are consistent with the Arctic Polynya observations of Barber et al. (2001). However, it should be noted that since weather conditions last seldom longer than a day in the polar region, it is difficult to directly compare Figure 2.6 with observations. For instance, the measurements of Brümmer and Schröder (2002) show that net heat flux can also be downward when the polynya is small.

The example of EMAD's response to the polynya condition reveals another difference between EMAD and previously used simple models, namely EMAD generates not only fluxes over the ice-free part of the ocean, but also fluxes over regions where sea-ice can be formed.

2.4.2 Second moment statistics

Section 2.4.1 considers only the stationary responses of EMAD. It does not indicate whether or not EMAD is able to realistically represent the second moment statistics of the time-varying part of the fluxes. This is studied in this section.

a) Variance distribution

The global distribution of the total variances produced by EMAD is considered first. For this purpose, EMAD is integrated in time using sea-surface conditions obtained from a 10-year integration with the ECHAM5/MPI-OM coupled model. The variances calculated from such an EMAD-integration are compared with those found in the same ECHAM5/MPI-OM integration (Figure 2.7). Also shown is the variance obtained from ECHO-G AO-GCM. EMAD reproduces the overall distribution, characterized by large wind stress variances at the mid-latitudes in both hemispheres. Notable differences from the coupled GCM-integrations are found with respect to the maxima. The maxima in EMAD are larger than those in the two coupled AO-GCM integrations. This is partly due to the fact that the ECHO-G model which is used to fit the EMAD-matrices produces somewhat larger variances than the ECHAM5/MPI-OM model.

However this fact alone does not completely explain the differences in maxima. There are two other possibilities which need to be considered. First, the SST data used to drive the EMAD may contain particular variations in the time-period of the integration chosen to drive EMAD, which could produce the larger maximum values. To clarify this, an additional EMAD integration is carried out, in which the $\mathcal{B}$-term is switched off. The variance of zonal wind stress produced by this EMAD integration is essentially identical to Figure 2.7a. This result rules out the possible effect of SST on the wind stress. The shape of the cross-correlation function between SST and wind stress, which will be shown next, also suggests that the SST does not contribute to wind stress in mid-latitudes. Secondly, the detailed implementation of the noise-term may also alter the magnitude of the variance. Let m be the number of EOFs of the residual part (i.e. the part which is not described by the $\mathcal{A}$ and $\mathcal{B}$ terms, see section 2.3.3). Ideally, the noise should be added for each flux in $\mathbf{x}$ using all m EOFs of the residual. In this case, one has $\mathcal{C}\mathbf{n} = \sum_{i=1}^{m} \mathbf{e}_i n_i$ with n_i being a zero-mean white noise whose variance equals the i-th eigenvalue of the covariance matrix of the residual. Since m is very large, the noise-term is implemented not using all the EOFs, but only the first 10. The variance explained by the remaining $m - 10$ EOFs are added together and represented by a single multivariate white noise. Such a representation, though easier to implement, does not

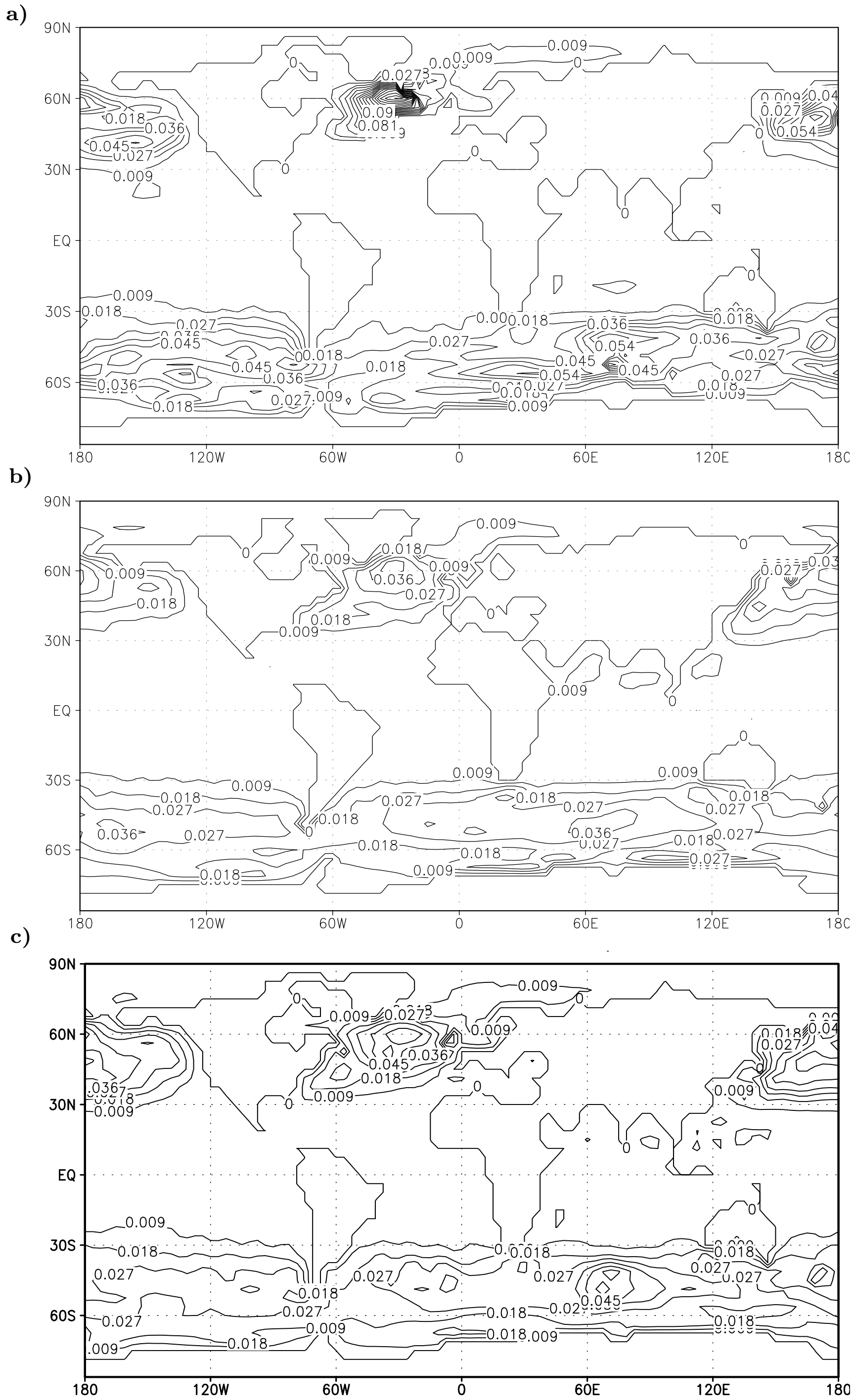

Fig. 2.7: Variances of the zonal wind stress (Pa^2) calculated from a) a 10-year integration of EMAD driven by the sea surface conditions obtained from a 10-year ECHAM5/MPI-OM integration, b) the same 10-year integration with the ECHAM5/MPI-OM model and c) a 10-year integration with the ECHO-G model.

ensure that the noise term has exactly the same covariance as the residual fluxes. The difference concerning the maximum values could be produced by such a noise implementation.

For the heat flux, the overall structure with the maximum over the Southern Ocean and western North Pacific and North Atlantic is reproduced by EMAD as well (Figure 2.8). Relative to ECHAM5/MPI-OM, the variance is larger in the EMAD run over most of the Southern Oceans, but smaller in the western North Pacific and western North Atlantic. Since the $\mathcal{B}$-term is important for the heat flux as is shown next (b), the differences in North Atlantic, North Pacific and Southern Ocean suggest that SST variations in MPI-OM are stronger in the North Atlantic and North Pacific and weaker in the Southern Ocean than those in HOPE-G. To test the role of the SST, an EMAD integration without the oceanic feedback term is carried out. A marked difference between fluxes from the EMAD integration with (Figure 2.8a) and without the $\mathcal{B}$-term (Figure 2.8c) underlines further the relevance of interaction between heat flux and SST. The mid- and high-latitudes over both hemispheres show less variance in EMAD fluxes when the $\mathcal{B}$-term is switched off. Due to the dominant role of SST in generating the variance of heat flux, the error induced by the noise implementation is less severe for heat flux than for wind stress.

Overall, despite some differences in the details, the general structures of the variances are reproduced by EMAD. The amplitudes are by and large comparable to those obtained from the ECHAM5/MPI-OM run.

b) Cross-correlation functions between SST and fluxes

In the EMAD run driven by the sea surface conditions from ECHAM5/MPI-OM, the SST anomalies are allowed to affect the fluxes, but the fluxes are unable to change the SST. To further check the interactions between the

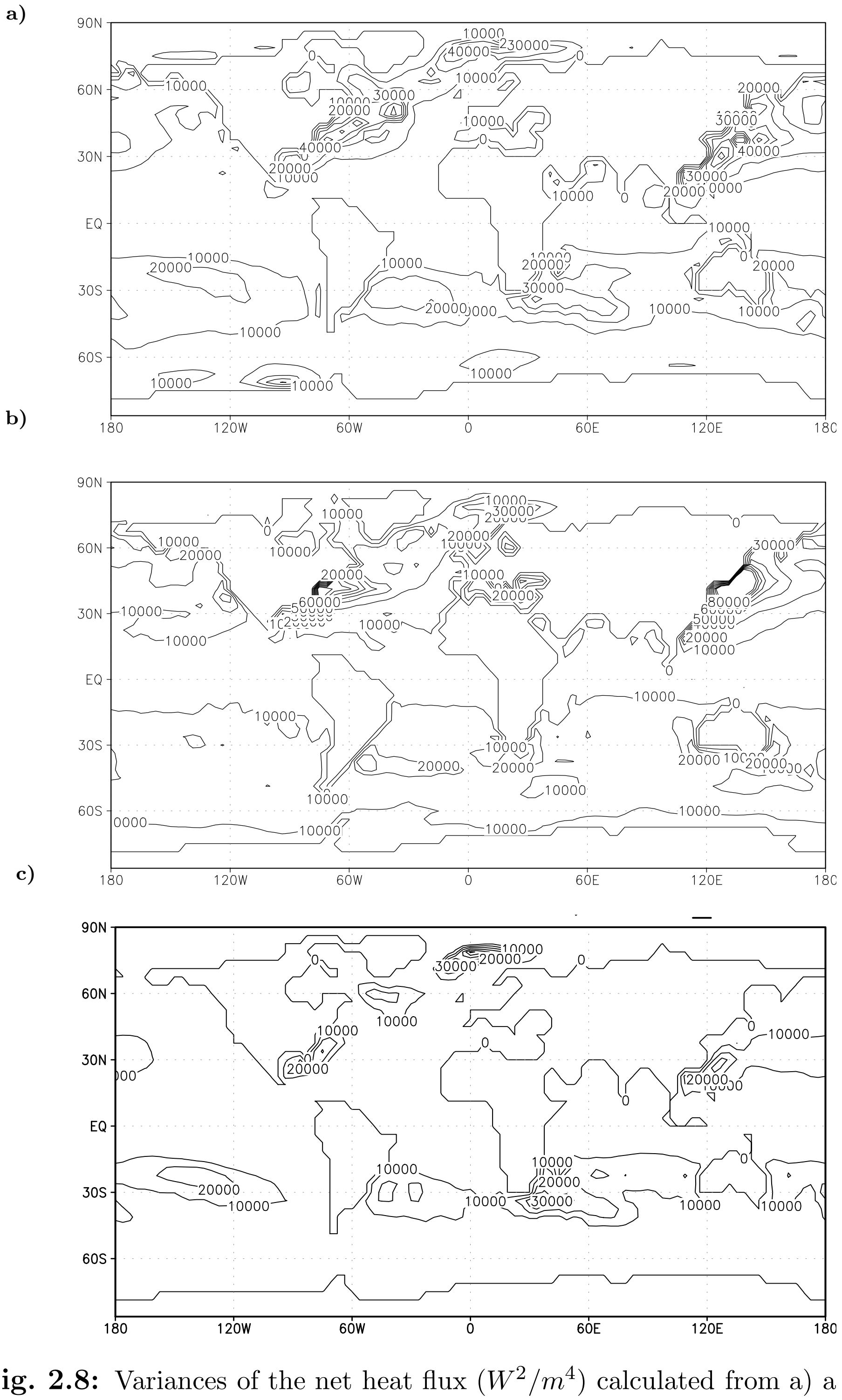

Fig. 2.8: Variances of the net heat flux (W^2/m^4) calculated from a) a 10-year integration of EMAD driven by the sea surface conditions obtained from a 10-year ECHAM5/MPI-OM integration, b) the same 10-year integration with the ECHAM5/MPI-OM model and c) a 10-year integration of EMAD without $\mathcal{B}$-term. Data more than 80000 W^2/m^4 over the western North Pacific is not plotted in b).

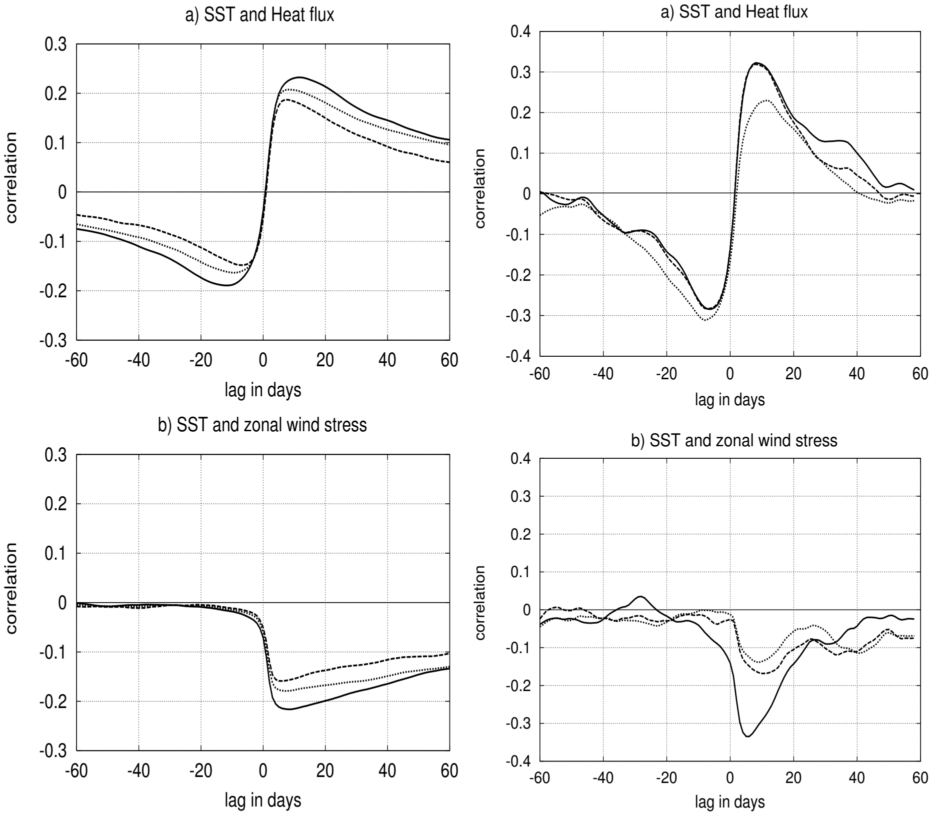

Fig. 2.9: Cross-correlation functions between SST and the net heat flux (top) and between SST and zonal wind stress (bottom) at three grid points which are located in the North Atlantic, North Pacific and South Pacific respectively. The correlation functions are derived from a 10-year EMAD/HOPE-G integration (right) and a 50-year ECHO-G integration (left).

fluxes and the sea surface conditions, EMAD is coupled to the HOPE-G O-GCM via OASIS (Valcke et al., 2000). Cross-correlations between SST and fluxes are calculated from a 10-year EMAD/HOPE-G integration and compared with those obtained from a 50-year-long time slice of the ECHO-G integration, that was not used to derive the EMAD.

Figure 2.9 shows the cross-correlation functions between SST and heat flux (top panel) and SST and zonal wind stress (bottom panel) at three extratropical grid points in the ECHO-G run (left) and at the same grid points in the EMAD/HOPE-G run (right).

The anti-symmetric shape of the cross-correlations between SST and the heat flux is characteristic over most part of the model ocean. It suggests that the heat flux acts to generate SST anomalies and these anomalies, once being generated, are damped by the heat flux. This type of interaction which cannot be described by a restoring condition as given in Eq.(2.1) is reproduced by the EMAD.

In the extratropical region, the interaction between SST and the zonal wind stress is characterized by the vanishing correlation between SST and wind stress when SST leads. This suggests that the feedbacks of SST anomalies to the wind stress are negligible. In other words, wind stress acts as a stochastic forcing for SST. This type of interaction, which cannot be described by Eq.(2.3), is reproduced by the EMAD.

2.5 Conclusions

This chapter introduces an empirical model which optimally represents the time-varying part of the fluxes at the sea surface. The model is based on the general structure given in Eq.(2.6) that allows different types of air-sea interactions, depending on the relative dominance of the model parameters. The parameters are fitted to a long time integration with the coupled ECHO-G model which parameterize the fluxes in a realistic (rather than ad hoc) manner. The such-derived model reacts to different sea surface conditions, produces variance distributions comparable to those obtained from a coupled AO-GCM, and reproduces characteristic air-sea interactions as suggested by the cross-correlation functions. The proposed empirical model can be updated when long and complete observational records or integrations with improved coupled AO-GCM are available. It can also be improved by taking the anomalies of other variables and forcing factors such as snow-depth and river run-off into consideration.

The present model differs from the previous simple models in various respects. It deals with all fluxes required to drive an O-GCM, rather than concentrating on one particular flux as in Eq.(2.1), Eq.(2.2), Eq.(2.3) and Eq.(2.4) outlined in section 2.1. It includes the time-varying part of fluxes which originate from both ocean and atmosphere. Furthermore, in contrast to the previous simple models which cannot deal with the sea-ice, the present model operates in regions where sea-ice can be formed and produces fluxes required to update the formation and melting of sea-ice. Finally, the present model allows different types of interactions to occur for different fluxes in different geographical regions, thereby allowing the reproduction of the air-sea interaction processes in a coupled AO-GCM.

This simple model, which is also computationally efficient, can be used in place of an A-GCM to drive an O-GCM. The validation of the model suggests that EMAD is capable of producing the basic features of the day-to-day flux anomalies. Using this linear anomaly model, one is able to assess the gross effect of the daily flux anomalies on the global circulation in the ocean.

Last but not the least, EMAD allows the separation of the effects of different air-sea interactions on the oceanic circulation. Such a separation is not possible with an A-GCM. This advantage of EMAD will be extensively used in this study.

3. COUPLED MODEL AND EXPERIMENTAL DESIGN

The atmospheric component of the coupled model used for this study is the empirical flux model, EMAD, which was described in the previous chapter. The ocean–sea-ice component and the numerical experiments conducted with the coupled model will be the theme of this chapter. A more complete description of the ocean model can be found in Marsland et al. (2003).

3.1 The ocean general circulation model: MPI-OM

The O-GCM used in the coupled system is the Max Planck Institute-Ocean Model (MPI-OM). It is a global model based on primitive equations for a Boussinesq fluid on a rotating sphere using a z-coordinate system. It is formulated on the horizontal Arakawa C-grid with the north pole located at northern Greenland and the south pole on the Antarctic continent. This grid configuration allows finer resolution over the Arctic ocean and high-latitude deep water formation sites as shown in Figure 3.1. The horizontal resolution varies from 20 km in the Arctic to about 350 km in the tropics.

For the present study, the model configuration with 40 vertical levels is used (Haak et al., 2003). 20 of these levels are in the upper 600m. The vertical resolution decreases with depth. The ocean topography is represented

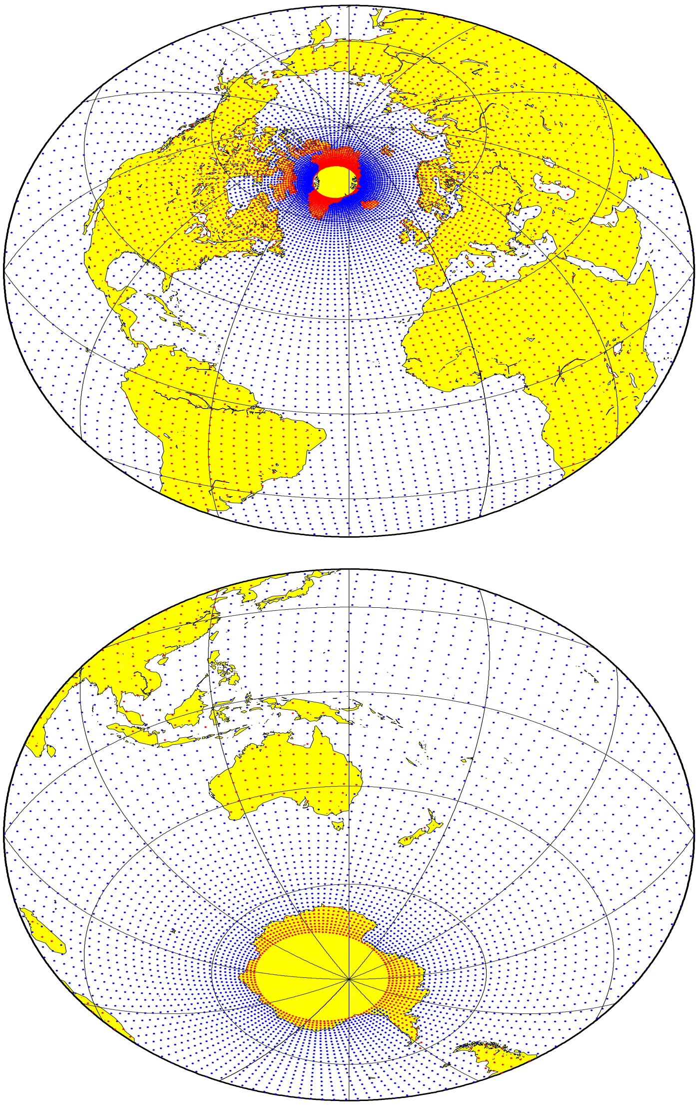

Fig. 3.1: Curvilinear orthogonal grid of the coarse resolution global version of MPI-OM used. The yellow circles over Greenland and Antarctica show the location of the shifted poles.

by the ETOPO-5 dataset interpolated to the model grid. The model contains partial bottom cells which helps to resolve the discretised topography more accurately. It allows a free ocean surface and treats sea-surface height as a prognostic variable. The horizontal velocity components are prognosed by the horizontal momentum equations. Vertical velocity is calculated by assuming incompressibility on the continuity equation. The tracers in this study are potential temperature and salinity. The tracer equation obeys an advection-diffusion balance and is given as

$$\frac{d\Theta}{dt} = \nabla_h \cdot \left(\mathcal{K} \nabla_h \Theta \right), \tag{3.1}$$

where Θ is potential temperature or salinity and ∇_h is the horizontal gradient operator. The tensor $\mathcal{K}$ describes the isoneutral and dianeutral diffusion and will be discussed in the next subsection. Density and pressure are diagnostic variables. Density is calculated from in-situ temperature, salinity and pressure using the UNESCO equation of state (UNESCO, 1983). Pressure is calculated diagnostically from the hydrostatic equation.

MPI-OM includes a sea-ice model with viscous-plastic rheology and snow. Sea-ice cover is fractional within grid cells and is related to sea-ice thickness. Sea-ice thickness changes in balance with different surface heat fluxes on the ice and with advection. For details of the dynamics and thermodynamics of the sea-ice model, see Marsland et al. (2003).

3.1.1 Subgridscale parameterisations

The processes which cannot be resolved within the grid-scale of the coarse resolution GCMs are represented in terms of known quantities or parameters. In the MPI-OM, subgridscale parameterisations describe the bottom boundary layer transport, convective events, mixing processes relevant for the thermohaline fields and friction associated with eddies.

A bottom boundary layer slope convection scheme is used in MPI-OM to represent the flow of statically unstable dense water over the sills and off continental slopes. Convection is parameterised as greatly enhanced vertical diffusion in the presence of static instability (Marotzke, 1991). Tracer diffusion is isoneutral and dianeutral and is described by the diffusion tensor $\mathcal{K}$ (Redi, 1982), which is a function of the neutral density gradient and horizontal and vertical diffusion coefficients K_H and K_V. The scheme is implemented numerically following Griffies (1998). The effect of horizontal tracer mixing by advection due to the unresolved mesoscale eddies is parameterized after Gent et al. (1995). The horizontal eddy viscosity is parameterized using a scale-dependent biharmonic formulation. The vertical eddy viscosity follows Pacanowski and Philander (1981). It utilizes an eddy coefficient which is represented in the same way as the vertical eddy diffusivity coefficient K_V in Eq.(3.2) below, except that the Richardson-number dependent part is proportional to $(1+C_{RD}R_i)^{-2}$, rather than $(1+C_{RD}R_i)^{-3}$ as in Eq.(3.3) below. The vertical diffusion coefficient K_V, plays an important role in the present study and deserves a more detailed discussion.

The vertical diffusion coefficient K_V is a function of convective mixing, Richardson-number (Ri) dependent mixing, wind-induced mixing and background diffusivity (Marsland et al., 2003). It is given by

$$K_V = \begin{cases} K_{conv} & \text{if statically unstable} \\ K_{Ri} + K_{wind} + K_{back} & \text{if statically stable.} \end{cases} \tag{3.2}$$

The Richardson-number dependent part equals

$$K_{Ri} = D_{VO}(1 + C_{RD}R_i)^{-3}, \tag{3.3}$$

where $D_{VO} = 2 \times 10^{-3}\ m^2s^{-1}$ and $C_{RD} = 5$ are model constants. According to Eq.(3.3), the maximum value of K_{Ri} is $2 \times 10^{-3}\ m^2s^{-1}$ for $Ri = 0$. The diffusion related to convection K_{conv} is set to $1 \times 10^{-1}\ m^2s^{-1}$. Thus, static instability is removed by switching on an extremely strong mixing. In the surface layer, the wind-induced mixing K_{wind} over ice free regions is given by

$$K_{wind} = W_T V_{10}^3, \tag{3.4}$$

where V_{10} is the local 10m wind speed and W_T is $5 \times 10^{-4}\ m^{-1}s^2$. Below the surface layer, K_{wind} depends on the stability of the water column and decays exponentially with an e-folding depth of 40 m. The diffusion related to other unresolved processes, such as internal waves, is described by $K_{back} = 10^{-5}$ m^2/s. This set of the parameters is used in the integration of MPI-OM coupled to the ECHAM5 A-GCM that produces a realistic oceanic state (Jungclaus et al., 2005) .

The vertical diffusion coefficient K_V can vary spatially and temporally, depending on the static stability and wind forcing. Generally, largest values of up to $10^{-2}\ m^2s^{-1}$ are found in the upper ocean above 900 m, while values decrease with depth to the order of $10^{-4}\ m^2s^{-1}$ below 2500 m. Like in many coarse resolution OGCMs, these values are probably too large compared to observations.

The net K_V is stored without separating the various contributions. This makes the identification of the various contributions to K_V difficult. Since K_{back} is unchanged in the experiments performed and since K_{wind} is confined to the first 40 meters of the ocean (depending on the stability), the changes in K_V below 40 meters are mainly related to the changes in K_{Ri} and / or K_{conv}.

Stochastically varying fluxes can change K_{conv} in a non-linear way by changing the stratification, thereby triggering or hampering convective mixing. The direction of the change depends on the background static stability. In the regions where the stratification is mostly stable and K_{conv} is mostly turned off, a positive buoyancy forcing makes the ocean more stable and will hence leave K_{conv} switched off. A negative buoyancy forcing, on the contrary, can reduce the static stability, causing K_{conv} to be switched on more often. The net effect is an increase in the convective mixing. Examples of mostly stable oceans are the tropical and subtropical oceans and the Pacific in the MPI-OM model. On the other hand, in regions where the stratification is mostly unstable and K_{conv} is mostly switched on, a negative buoyancy forcing will not affect the convective mixing too much, since the convective mixing is already switched on. A positive buoyancy anomaly on the contrary can increase the static stability, causing K_{conv} to be switched on less often. The net effect is a decrease in K_V. Examples of mostly unstable oceans are the GIN (Greenland-Iceland-Norwegian) Sea and the high-latitude Southern Ocean in the MPI-OM model. Given the mean stratification in the MPI-OM model, changes in convective mixing due to fluctuations are expected to be characterized in the Southern Ocean by a latitudinal dipole structure with enhanced mixing in the subtropics and mid-latitudes and reduced mixing in the high-latitudes. In the North Atlantic, the changes in convective mixing due to fluctuations are expected to be characterised by enhanced mixing in the subtropics and reduced mixing in the GIN sea.

Fluctuating fluxes can also change the Ri-dependent mixing, since anomalous buoyancy forcing at the sea surface can affect the stratification of the water column and anomalous wind stress can alter the shear of the current. The change in the Ri-dependent mixing is expected to be more pronounced in the tropics. In these regions, the static stability of the ocean is so high that static instability rarely occurs and, when it occurs, it is confined to a shallow surface layer.

Apart from the stochastic fluctuating fluxes, the SST-feedback can also change the Ri-dependent mixing and the convective mixing by modifying the stratification. It will be shown in the following chapter that the SST-feedback leads to a reduction in SST in the GIN Sea and in the high-latitude Southern Ocean. This makes the ocean less stable there, hence allowing an increase in both K_{Ri} and K_{conv}.

3.2 The coupled model: EMAD/MPI-OM

An A-GCM in a coupled AO-GCM produces both the climatological and the time-varying components of the fluxes at the cost of heavy computations. EMAD produces time-varying components at almost no additional computational costs. Also, no coupler is needed to exchange the variables describing the coupling because direct coupling is used to couple EMAD with MPI-OM. The procedures and data fields required for the coupling are shortly described below.

a) Variables used for the coupling

The MPI-OM ocean model requires momentum, freshwater and heat fluxes over open water and momentum, freshwater and conductive and residual heat fluxes over sea-ice. Apart from that, it also requires 10m wind speed and solar radiation. The 10m wind speed is needed for the near surface wind mixing. The solar radiation is needed for its downward penetration into the ocean. All fluxes and solar radiation are included in $\mathbf{x}'$ of Equation (2.6). The 10m windspeed is derived from the momentum flux using the bulk formula. EMAD, on the other hand, requires SST, sea-ice cover and sea-ice thickness.

b) Grid transformation needed for the coupling

A bilinear interpolation is used to transform the scalar and vector data from T30 atmospheric grid to the curvilinear ocean grid and vice-versa. For vector variables, an additional rotation is needed. In the curvilinear grid, the zonal and meridional components of vector data do not lie along the true east-west and north-south directions, respectively. For this reason,

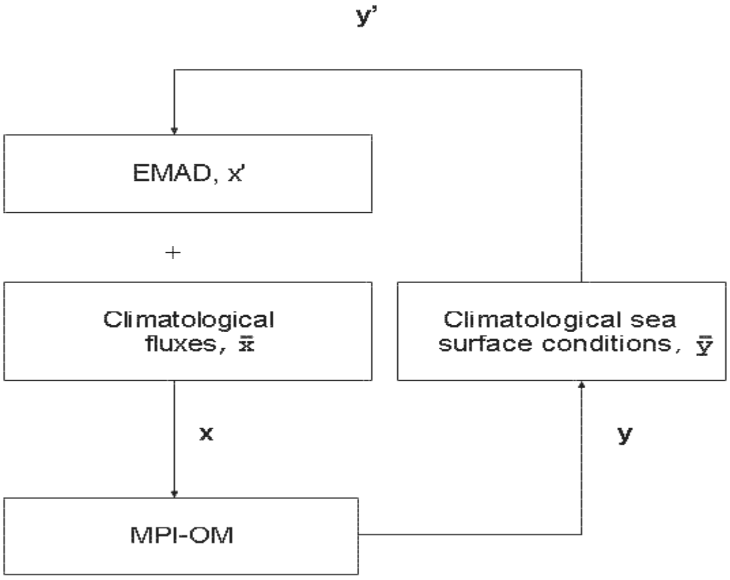

Fig. 3.2: Schematics of the coupling of EMAD to MPI-OM.

before passing to the ocean, the zonal and meridional components of the momentum flux vectors are rotated in order to place them on the orthogonal meridians and parallels of the ocean grid.

c) Climatological mean fields needed for the coupling

When coupling EMAD to the MPI-OM, one also needs a set of fields of climatological mean fluxes, mean 10m wind speed, mean solar radiation and a set of fields of climatological mean sea surface conditions. These climatological mean data are derived from the last 50 years of a 600-year integration with the ECHAM5/MPI-OM coupled AO-GCM (Jungclaus et al., 2005). The climatology contains the annual cycle with a one-day resolution.

d) The coupling

The coupling is described in Figure 3.2. Given an oceanic state $\mathbf{y}$ at time t, the anomalous sea surface condition $\mathbf{y}^{'}$ is derived by subtracting the actual oceanic state from the given climatological mean state. With this $\mathbf{y}^{'}$ and the anomalous flux forcing $\mathbf{x}^{'}$ at $t-1$, EMAD produces the anomalous flux forcing at t. Adding this to the climatological mean forcing $\bar{\mathbf{x}}$ gives the net flux forcing $\mathbf{x}$ at time t which is used to produce $\mathbf{y}^{'}$ at time $t+1$. The coupling takes place once a day.

e) Procedure needed to keep the coupled system in the desired mean state

Apart from the feedbacks described by $\mathcal{B}$ in Equation (2.6), there is no relaxation of salinity or temperature in the ocean. The only procedure used to prevent the ocean drifting away from the given climatological mean state is to restore the sea-ice cover and sea-ice thickness to that found in the integration with the ECHAM5/MPI-OM. The restoring time constant is 39 days.

3.3 Numerical experiments

Various numerical experiments were performed to study the effect of different types of air-sea fluxes on the oceanic circulation. To isolate the effect of the daily flux anomalies from the climatological mean fluxes, two experiments are necessary. In the first one, referred to as experiment CLIM, MPI-OM was forced with the climatological mean fluxes obtained from the ECHAM5/MPI-OM integration. In the second one, referred to as experiment ABC which includes all the three terms in Eq.(2.6), the MPI-OM was forced with the same climatological mean fluxes plus anomalous fluxes produced by EMAD. The difference between the two experiments describes the total effect of day-to-day flux anomalies.

To further understand the effect identified by the difference between experiments CLIM and ABC, three additional experiments were performed. A pronounced difference between experiments ABC and CLIM is that the tropical SST in CLIM is unrealistically warm, while the SST in ABC is comparable to observations and to that found in the coupled ECHAM5/MPI-OM integration. To understand how this happens, experiment BH was carried out. Here, MPI-OM was driven by the same climatological mean fluxes of heat, freshwater and momentum as in experiment CLIM, plus an additional heat flux anomaly $H^{'}$, which was obtained from $\mathcal{B}\mathbf{y}^{'}$ with $\mathbf{y}^{'}$ representing SST anomaly. It will be shown later that this SST-feedback on heat flux significantly reduces deviations of SST from the given climatological mean values, making the SST field and from that the surface density field in experiment BH comparable to the respective fields in experiment ABC. Experiment BH, in particular the difference between BH and CLIM, can be used to identify the role of SST-feedback on heat flux.

In a further experiment, referred to as AC, MPI-OM was coupled to a version of EMAD with the feedback term $\mathcal{B}\mathbf{y}^{'}$ switched off. The fluxes became purely stochastic and independent of the oceanic state. With experiment AC, the effect of stochastic fluctuations in the absence of oceanic feedback can be isolated. As the SST-feedback on heat flux is absent, the SST in AC differs significantly from that in ABC and is close to that in CLIM.

In principle, the effect of fluctuating fluxes can be described by considering the difference between AC and CLIM. However, since both AC and CLIM do not contain the oceanic feedback on heat flux, the tropical SST in these two experiments are too high. Consequently, the oceanic state in experiments AC and CLIM differs significantly from the state in ABC. Given different oceanic states, it is possible that the effect of fluctuating fluxes in the absence of feedback is different from that in the presence of feedback.

name	fluxes used	characteristics
CLIM	$\bar{\mathbf{x}}$	no fluctuations, no feedback
BH	$\bar{\mathbf{x}}+\mathbf{x}'$ $\mathbf{x}_t' = \mathcal{B}\mathbf{y}_t', \quad (\mathbf{x}' = H', \mathbf{y}' = SST')$	no fluctuations, with SST-feedback on heat flux
ABC	$\bar{\mathbf{x}}+\mathbf{x}'$, $\mathbf{x}_t' = \mathcal{A}\mathbf{x}_{t-1}' + \mathcal{B}\mathbf{y}_t' + \mathcal{C}\mathbf{n}_t$	with fluctuations + feedback
AC	$\bar{\mathbf{x}}+\mathbf{x}'$, $\mathbf{x}_t' = \mathcal{A}\mathbf{x}_{t-1}' + \mathcal{C}\mathbf{n}_t$	no feedback, with fluctuations
AB2C	$\bar{\mathbf{x}}+\mathbf{x}'$, $\mathbf{x}_t' = \mathcal{A}\mathbf{x}_{t-1}' + \mathcal{B}\mathbf{y}_t' + 2 \times \mathcal{C}\mathbf{n}_t$	with feedback + 2× fluctuations

Tab. 3.1: Experiments done with MPI-OM and different versions of EMAD model. $\bar{\mathbf{x}}$ denotes the climatological fluxes and $\mathbf{x}'$ the flux anomalies produced by different versions of the EMAD model.

This possibility is studied using the final experiment AB2C, in which MPI-OM was coupled to EMAD with oceanic feedback, but with the variance of white noise being doubled. With experiment AB2C, the effect of fluctuating fluxes in the presence of oceanic feedback can be justified further.

The five experiments are summarized in Tab.3.1. For each experiment, a spin-up run of a few hundred years was carried out. The spin-up runs started from the same initial state obtained from the coupled ECHAM5/MPI-OM (Jungclaus et al., 2005), after the ocean has reached a more or less statistically stationary state. Following the respective spin-up runs, the experiments were carried out for 200 years. The analysis given below is based on these 200-year integrations.

EMAD is used to identify effects of various components in the daily fluxes. This can neither be done with a coupled AO-GCM nor with observations. By doing the experiments, one deals with idealised situations, which are not comparable to observations. However, the results of experiment ABC can be compared to observations or other AO-GCM studies in the sense that daily flux anomalies which drive the O-GCM in this case are optimally equivalent to that from an A-GCM.

Note that the time-mean fluxes are essentially the same in all experiments. Obviously, the mean fluxes in experiment CLIM are equal to the chosen climatological flux forcing. In the absence of the $\mathcal{B}$-term (i.e. in experiment AC), $\mathbf{x}'$ produced by Eq.(2.6) has a zero time-mean by construction so that the mean fluxes are identical to those in experiment CLIM. In the presence of the $\mathcal{B}$-term (i.e. in experiment BH, ABC, AB2C), the time mean of $\mathbf{y}'$ and from that $\mathbf{x}'$ would essentially be zero, if the time-mean sea surface condition obtained from EMAD/MPI-OM is about the same as that obtained from ECHAM5/MPI-OM. In general, the global mean SST in experiments with the $\mathcal{B}$-term is by and large comparable to that in ECHAM5/MPI-OM. Locally, there are some discrepancies between the SST in the EMAD/MPI-OM run and that in the ECHAM5/MPI-OM run. Probably due to these discrepancies, there is a northward shift of the mean zonal wind stress pattern over the Southern Ocean by about three to five degrees. However, the maximum values of the zonal wind-stress have the same magnitude of 0.25 to 0.3 Pa over the Indian Ocean sector of the Southern Ocean in both EMAD/MPI-OM and ECHAM5/MPI-OM.

Having now outlined the tool and the experimental set-up used in this study, in the next chapter, the results of the various experiments are presented.

4. EFFECT OF DAILY SURFACE FLUXES ON THE TIME-MEAN OCEAN

The focus of this chapter is on the results of the numerical experiments done with the coupled EMAD/MPIOM. The model results show that the day-to-day flux anomalies do have a considerable effect on the time-mean circulation of the ocean (Beena and von Storch, 2006). The first section mainly deals with the time-mean changes in different oceanic variables caused by the daily flux anomalies. A discussion of the specific roles of the stochastically fluctuating part and the oceanic feedback part of the daily flux anomalies is given in the second section.

4.1 Changes induced by day-to-day flux anomalies

4.1.1 Time evolution

This subsection describes the time evolution of the oceanic states produced by different types of daily fluxes. The consideration is confined to the globally integrated sea surface temperature (SST) and two circulation indices, namely the MOC-index and the Drake Passage mass transport. The globally integrated SST is considered to describe the effect of the SST-feedback over time. The MOC-index and the Drake Passage mass transport are chosen since they characterize global-scale circulation in the ocean. The time

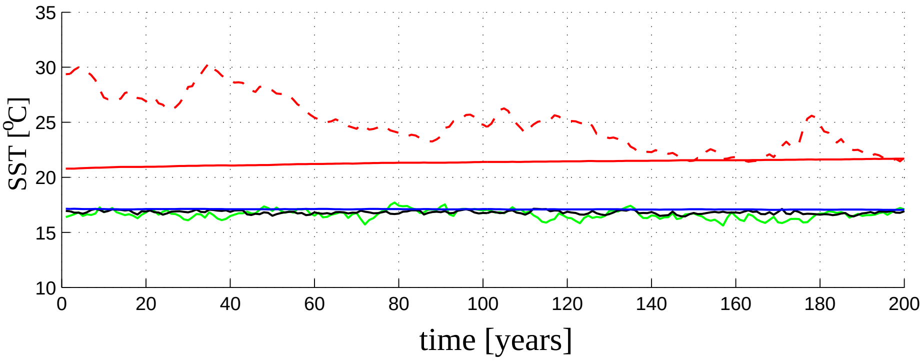

Fig. 4.1: Time series of globally integrated surface temperature in ^oC . The lines indicate experiments CLIM (red solid), BH (blue), ABC (black), AC (red dashed) and AB2C (green).

series also indicate the changes in variability that are caused by different types of flux anomalies. These changes are only briefly discussed and the main focus remains on the changes in the time-mean state, as in the other subsections.

Figure 4.1 shows the yearly time series of globally integrated SST for various experiments. In experiments BH (blue), ABC (black) and AB2C (green), in which the SST-feedback on the heat flux is present (i.e. in all experiments with label B), the SST time series are essentially statistically stationary and have roughly the same mean value of about $17°C$. In experiments CLIM (red solid) and AC (red dashed) on the contrary, the SST curves suggest much too warm climates. The absence of SST-feedback on heat flux is expected to lead to an increase in SST in the tropics where the net heat flux is positive (i.e. downward) and a decrease in SST in the mid- and high-latitudes where the net heat flux is negative (i.e. upward). However, only the SST in the tropics can increase without bound. The decrease in the mid- and high-latitudes is limited by the freezing temperature. This has the consequence that the warming in the tropics dominates the cooling in the extra-tropics.

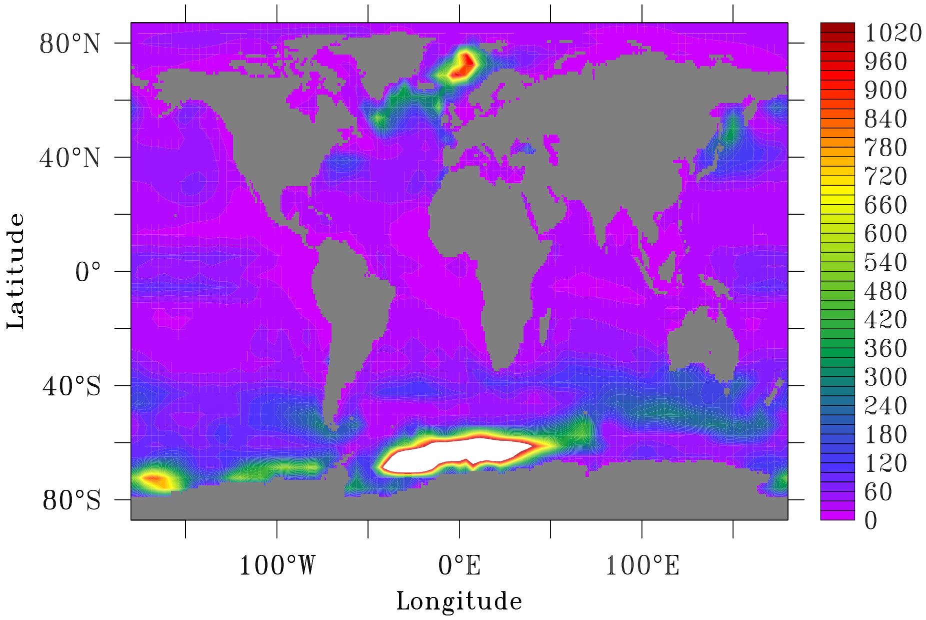

Fig. 4.2: Mean mixed layer depth (meters) in experiment ABC. Shading interval is 20m and colors are labelled every three intervals. The white area indicates values larger than 1040m.

The warming is further enhanced due to the fact that the model mixed layer depth is much shallower in the tropical and subtropical oceans relative to that in the high-latitudes of the Southern Ocean, in the northern North Atlantic and in the northwest Pacific (Figure 4.2). The difference in mixed layer depth makes the heating effect of the downward heat flux more effective in the tropics than the cooling effect in the extratropics.

To further rule out the possibility that the warming results from the imbalance in the net heat flux, the global integral of the climatological mean heat flux used in experiment CLIM as well as in other experiments is calculated. The global integral of the climatological heat flux is about -0.07 PW (corresponding to -0.2 W/m^2), which should induce a decrease, rather than an increase, in globally integrated SST. This suggests that the too high SSTs in CLIM and AC are caused by the lack of oceanic feedback in conjunction with the limitation by the freezing temperature and shallow mixed

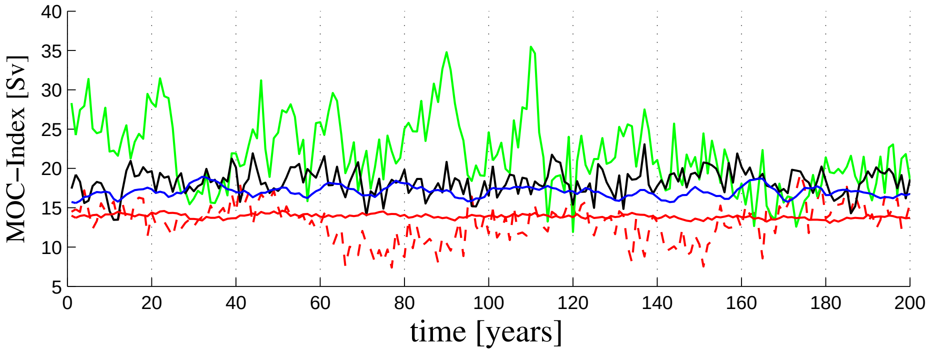

Fig. 4.3: Time series of the maximum of Atlantic meridional overturning streamfunction located at 30°N in Sv (MOC-index). The lines indicate experiments CLIM (red solid), BH (blue), ABC (black), AC (red dashed) and AB2C (green).

layer depth in the tropics, rather than by the imbalance in the globally integrated heat flux. Another outstanding feature of Figure 4.1 is the much stronger SST-variability obtained in experiment AC (red dashed) relative to experiments ABC (black) and AB2C (green). The variations are mostly on multidecadal and centennial time scales. In fact, the downward trend in the SST in experiment AC shown by the red dashed line in Figure 4.1 is a part of low frequency variation which is not resolved by the 200 years of the time series. Even though stochastic fluctuations excite a notable amount of SST variability, the excitation is much less efficient in the presence of SST-feedback.

Figure 4.3 shows the time series of the MOC-index, defined as the maximum of the Atlantic overturning streamfunction at 30°N around 1000m depth. The experiment CLIM (red solid), which does not include fluctuating fluxes, reveals little variability in the MOC. The presence of the SST-feedback in experiment BH (blue) leads to some decadal variations. Stronger variations are obtained by including fluctuations. The variations are strongest, in particular on multidecadal time scales, in experiment AB2C (green) where the variance of the stochastic forcing is doubled. In exper-

a) MOC [Sv]

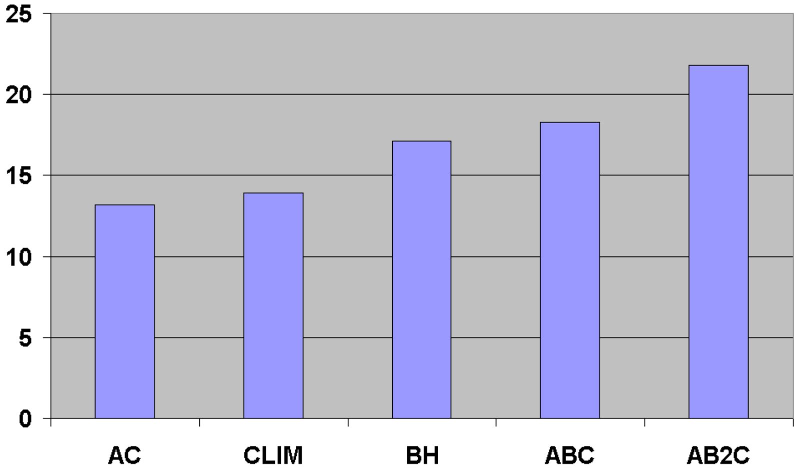

b) ACC [Sv]

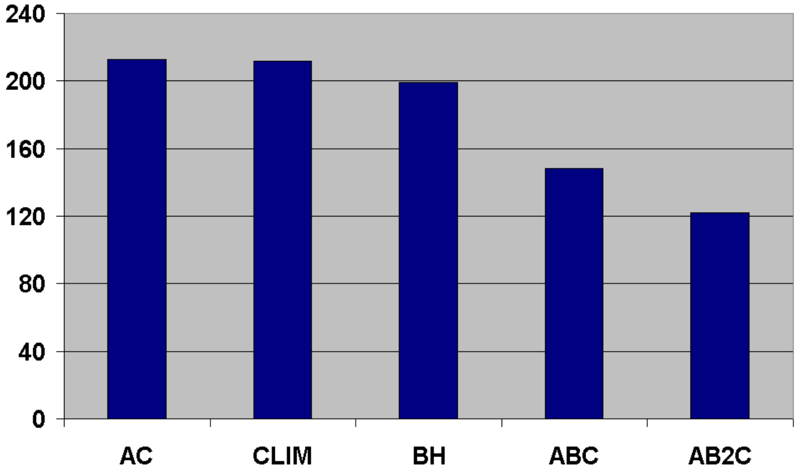

Fig. 4.4: 200-year means of a) MOC-index and b) Drake Passage transport in Sv in different experiments.

iments ABC (black) and AC (red dashed), which operate with the same amount of stochastic forcing, much stronger low-frequency variations are obtained from AC when the SST-feedback is absent. The SST-feedback seems to hamper the variability in the MOC, as in the case of the SST.

Not only the variability, but also the time mean of the MOC-index changes from experiment to experiment. This is further demonstrated in

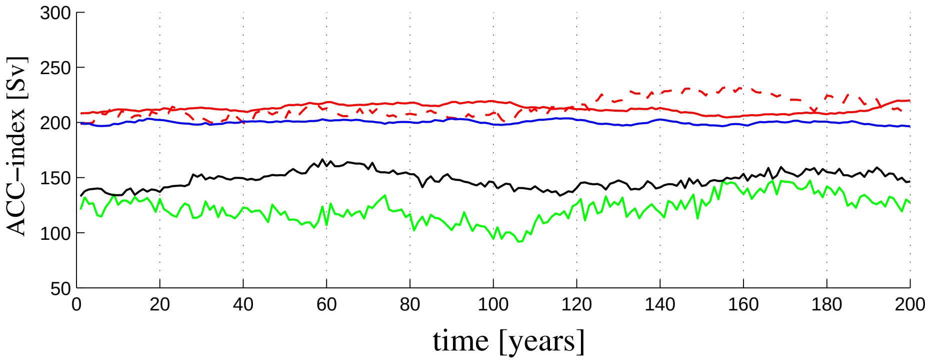

Fig. 4.5: Time series of Drake Passage mass transport in Sv (ACC-index). The lines indicate experiments CLIM (red solid), BH (blue), ABC (black), AC (red dashed) and AB2C (green).

Figure 4.4a. The smallest mean value of about 13 to 14 Sv is obtained from experiments AC and CLIM, in which the SST-feedback is absent. By including the SST-feedback in experiment BH, the value increases to about 17 Sv. Inclusion of fluctuations leads to a further increase to about 18 Sv in experiment ABC. The strongest MOC of about 22 Sv is obtained when the SST-feedback is at work and the stochastic forcing is doubled.

Figure 4.5 shows the time series of the mass transport through the Drake Passage calculated from the difference of barotropic streamfunction between two land points bordering the Passage. The variations of the transport are much weaker on decadal to interdecadal time scales relative to those in the MOC. There is an enhancement of variability through fluctuations in experiment AC, ABC and AB2C. The presence of the SST-feedback does not significantly affect the variability in the Drake Passage transport.

Concerning the time-mean (see also Figure 4.4b), a too strong mean transport of about 200 to 210 Sv is obtained in experiments BH, CLIM and AC. The transport reduces to about 147 Sv in experiment ABC and to about 122 Sv in AB2C.

A comparison of Figure 4.4b with Figure 4.4a suggests that a stronger overturning circulation is related to a weaker Antarctic Circumpolar Current. The relation concerns only the time-mean values. The variability of the Drake Passage transport is not correlated to that of the MOC-index.

4.1.2 Changes in the circulation pattern

The different types of flux anomalies at the sea surface produce not only changes in the strength of the circulation, which is characterized by the MOC-index (Figure 4.3 and Figure 4.4a) and the Drake Passage transport (Figure 4.5 and Figure 4.4b), but also changes in the structure of the circulation. When MPI-OM is driven with climatological fluxes without oceanic feedback, the Atlantic overturning cell is weak and shallow (Figure 4.6a). A similar overturning circulation is obtained in experiment AC (Figure 4.6b). The overturning cell becomes notably stronger and extends a couple of hundred meters deeper into the deep ocean in experiment BH, in which the SST-feedback is included (Figure 4.6c). Relative to CLIM and AC, the overturning cell in BH is much closer to that in experiment ABC (Figure 4.6d). It is, however, still somewhat weaker than that in ABC, indicating that the fluctuating fluxes also play a role in determining the MOC. When the stochastic forcing is doubled, the overturning circulation strengthens and deepens further (Figure 4.6e). The deepening of the overturning cell is accompanied by the weakening of the Antarctic Bottom Water cell and the retreat of Antarctic Bottom Water (AABW). In experiment AB2C, the penetration of AABW into the abyssal North Atlantic is severely blocked.

The changes described by the Drake-Passage transport reflects the changes in the Antarctic Circumpolar Current over a broad latitudinal band of the Southern Ocean. This is further demonstrated by the barotropic zonal velocity (Figure 4.7). There is a clear reduction of the eastward zonal velocity in the Southern Ocean from experiments without fluctuating fluxes (i.e.

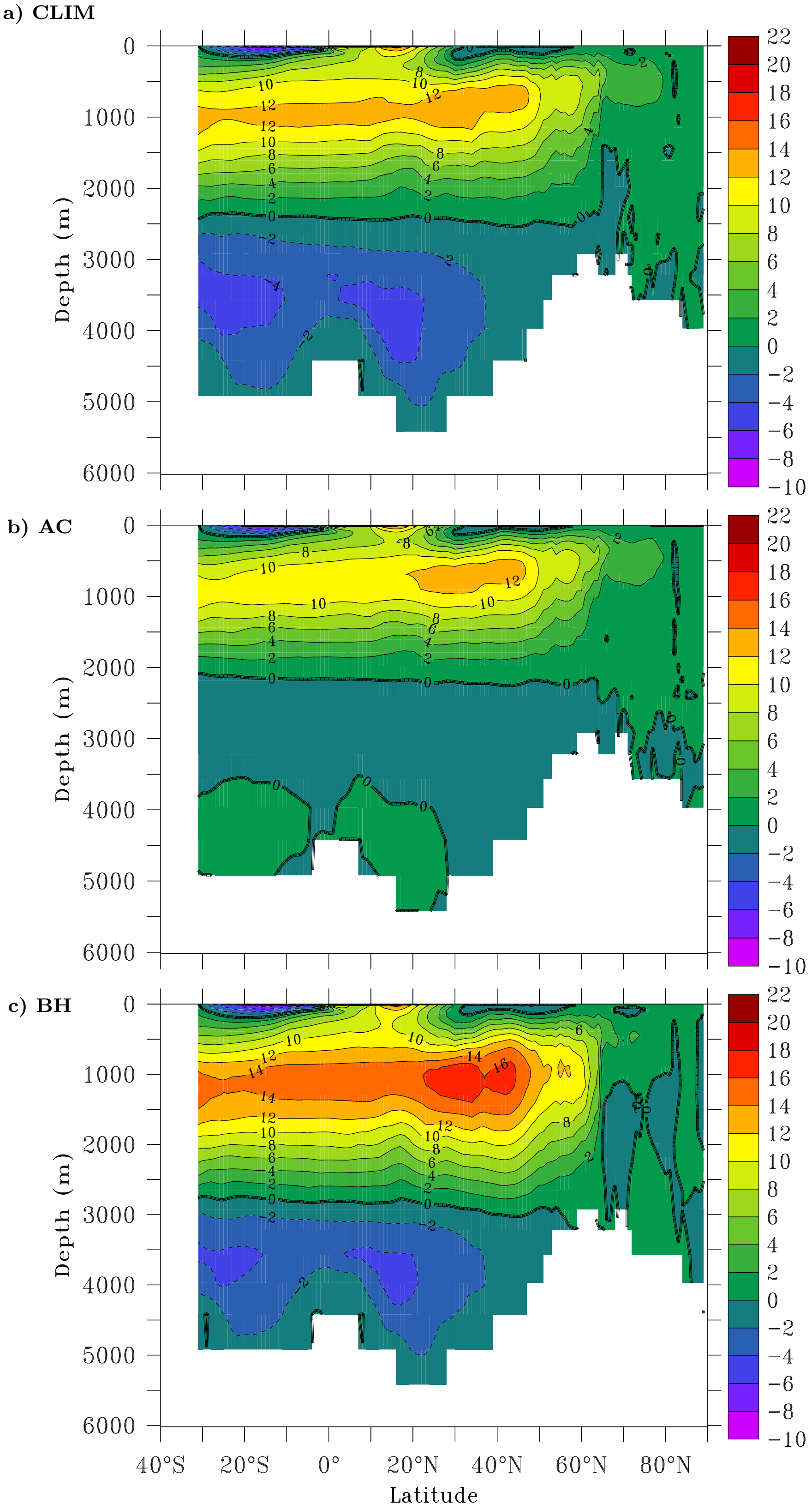

(to be continued...)

d) ABC

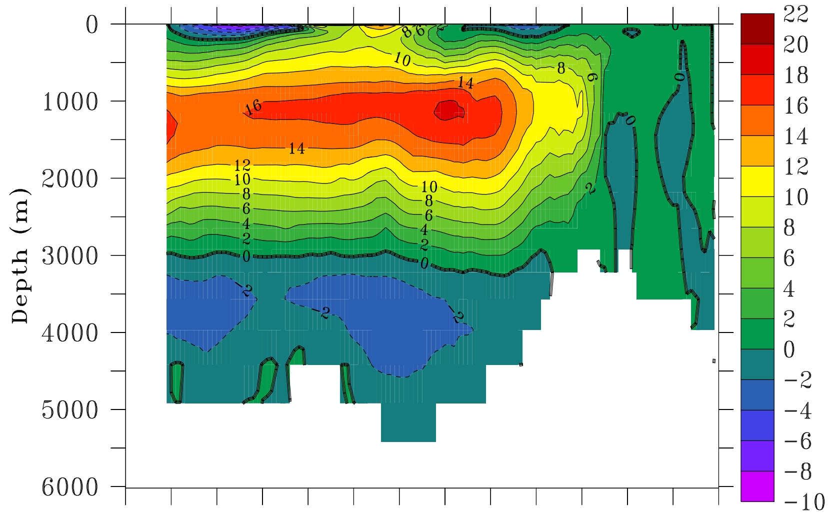

e) AB2C

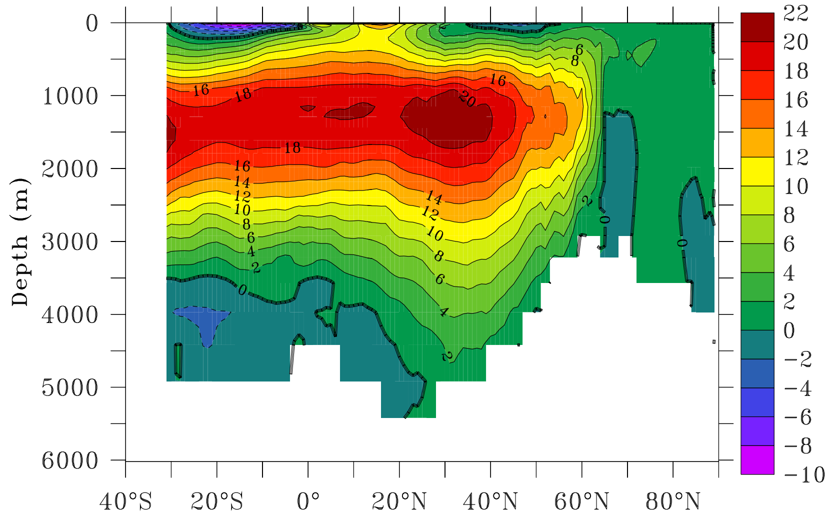

Fig. 4.6: (continued from previous page) Spatial structure of the time-mean Atlantic MOC in Sv in different experiments.

a) CLIM

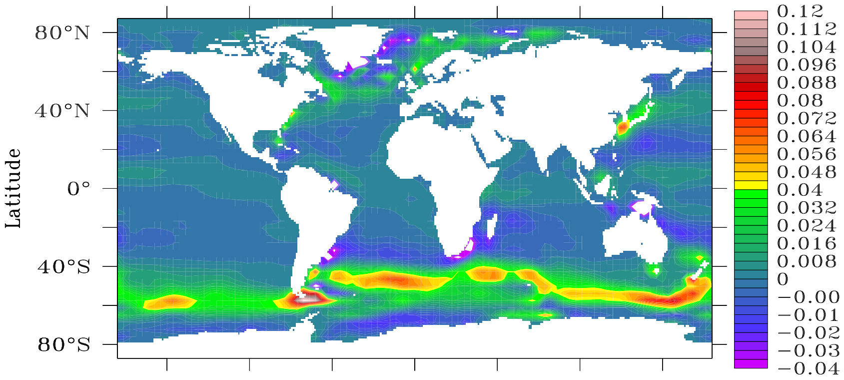

b) BH

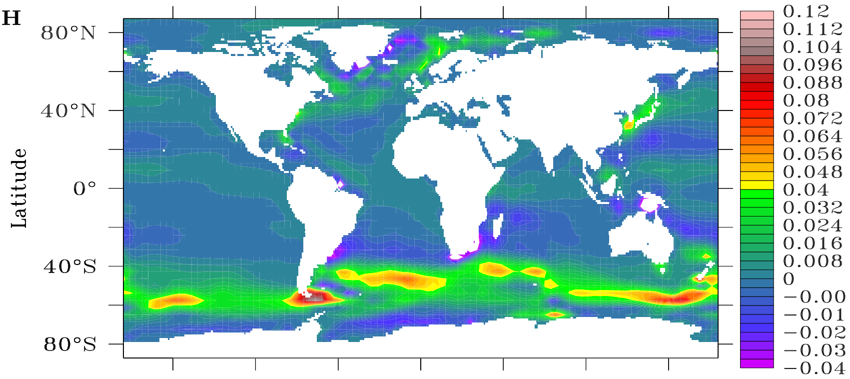

c) ABC

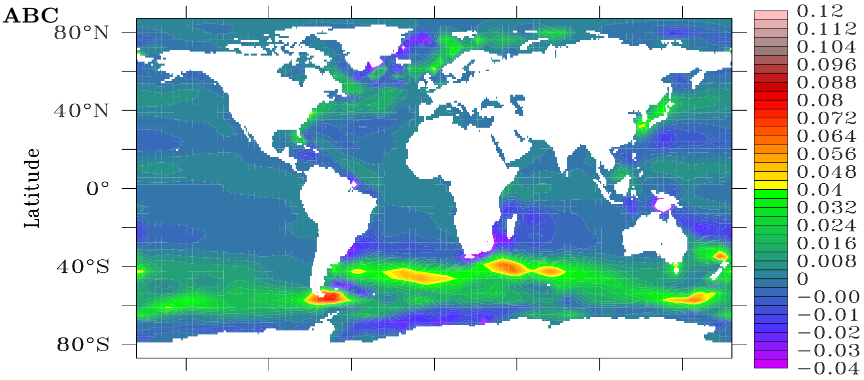

d) AB2C

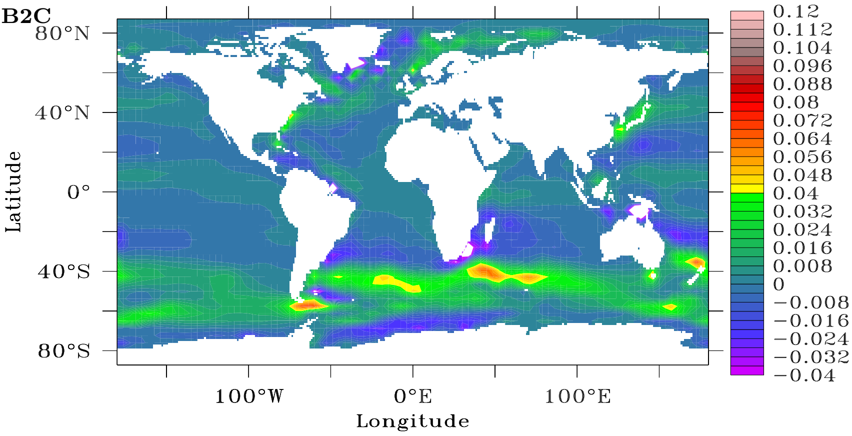

Fig. 4.7: Horizontal distribution of zonal barotropic velocity in m/s in different experiments. Colors are labelled every two intervals.

CLIM, BH) to experiment ABC with fluctuating fluxes, and further to experiment AB2C with stronger fluctuations. A reduction of the zonal current is also found in the region of Kuroshio.

4.1.3 Changes in the density fields

Changes in the circulation are related to changes in the density fields. To understand the latter, changes in the SST and sea surface salinity (SSS) are considered first. The pronounced feature of the SST-fields obtained from different experiments (Figure 4.8) is the much too high SSTs in experiment CLIM relative to the SST in experiments BH, ABC and AB2C. As pointed out in subsection 4.1.1, this warming results from the lack of SST-feedback on the heat flux. The tropical ocean is warmed drastically by a constant supply of heat. The cooling in the extra-tropical ocean due to constant outgoing heat flux is limited by the freezing temperature. Together with the fact that the mixed layer depth in the tropical and subtropical ocean is shallower than that in the high-latitudes, the warming dominates the cooling. A similar SST-distribution is also found in experiment AC (not shown). These unrealistic SSTs in experiments CLIM and AC are corrected by taking the SST-feedback into account in experiment BH. The SST-field in experiment BH is very close to that in experiment ABC. When the stochastic forcing is doubled, the warm pool in the western Pacific becomes somewhat cooler, while the eastern Pacific warms.

Figure 4.9 shows fields of sea surface salinity (SSS) obtained in different experiments. The inclusion of SST-feedback reduces the salinity maximum in the subtropical Atlantic from maximum values of about 38 psu in experiment CLIM (Figure 4.9a) to values of about 37.5 psu in experiment BH (Figure 4.9b). North of this salinity maximum, there is a salinity minimum. This minimum is weakened in experiment ABC (Figure 4.9c). When the

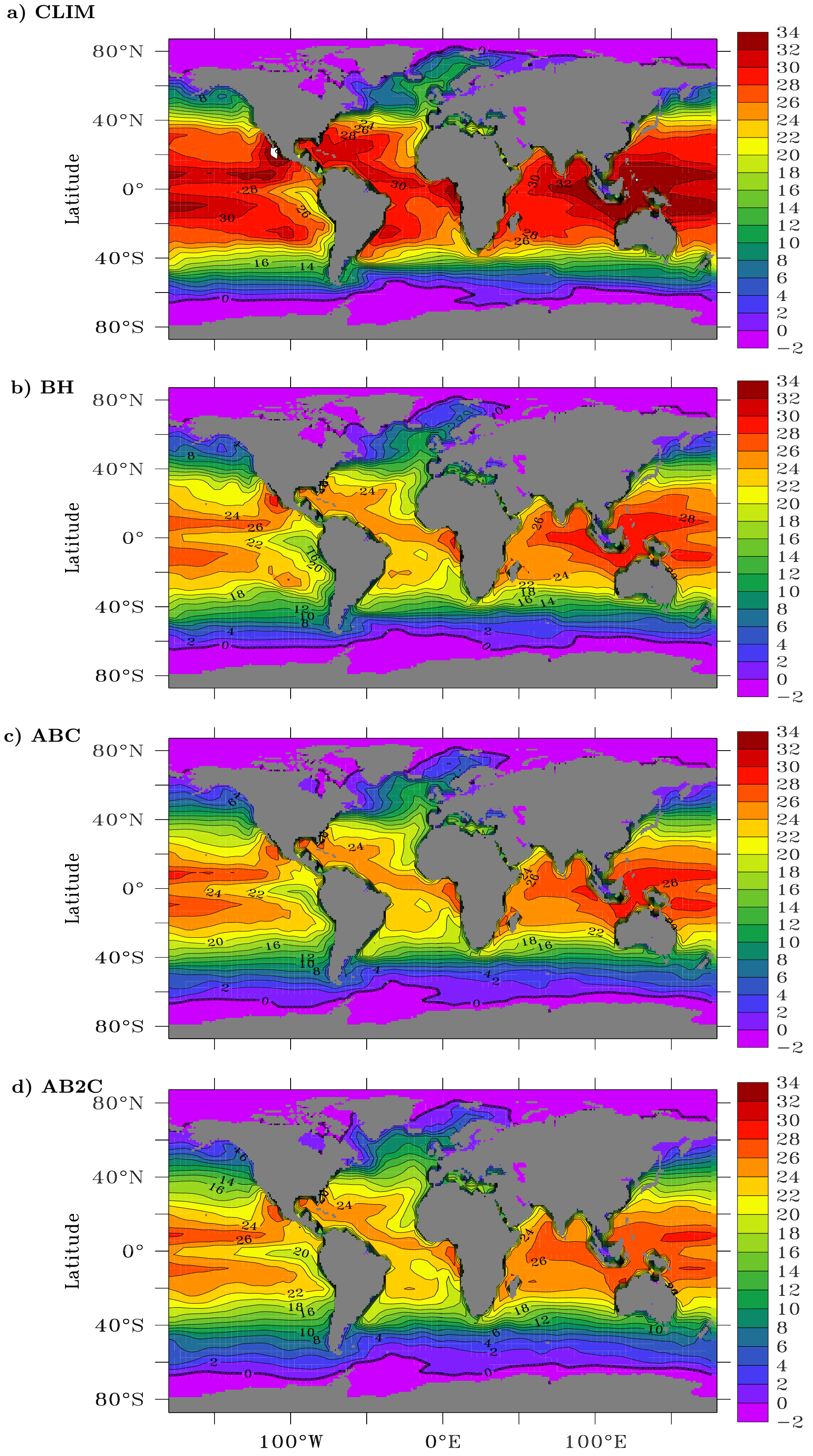

Fig. 4.8: Horizontal distribution of sea surface temperature in ^oC in different experiments.

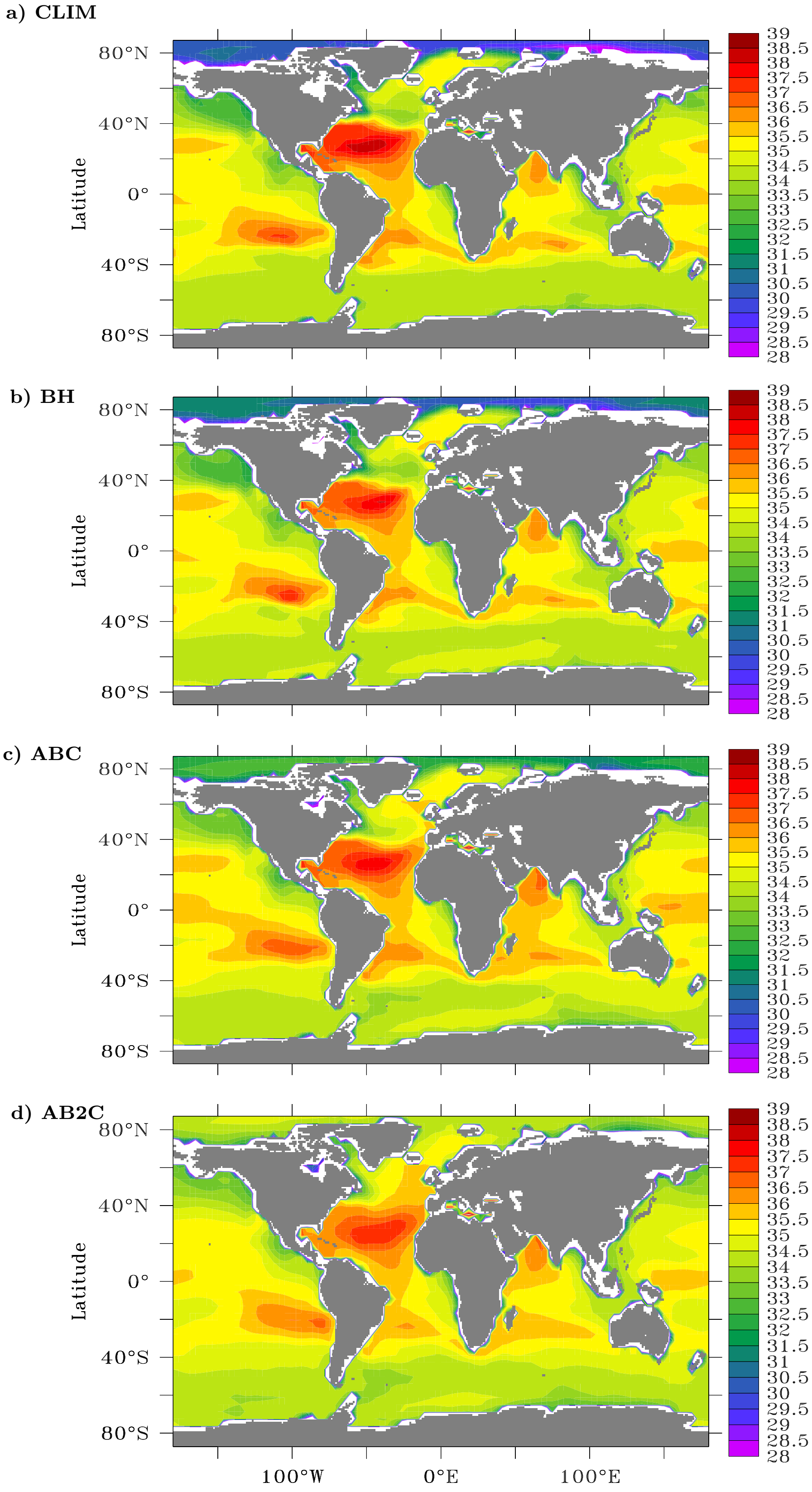

Fig. 4.9: Horizontal distribution of sea surface salinity in *psu* in different experiments.

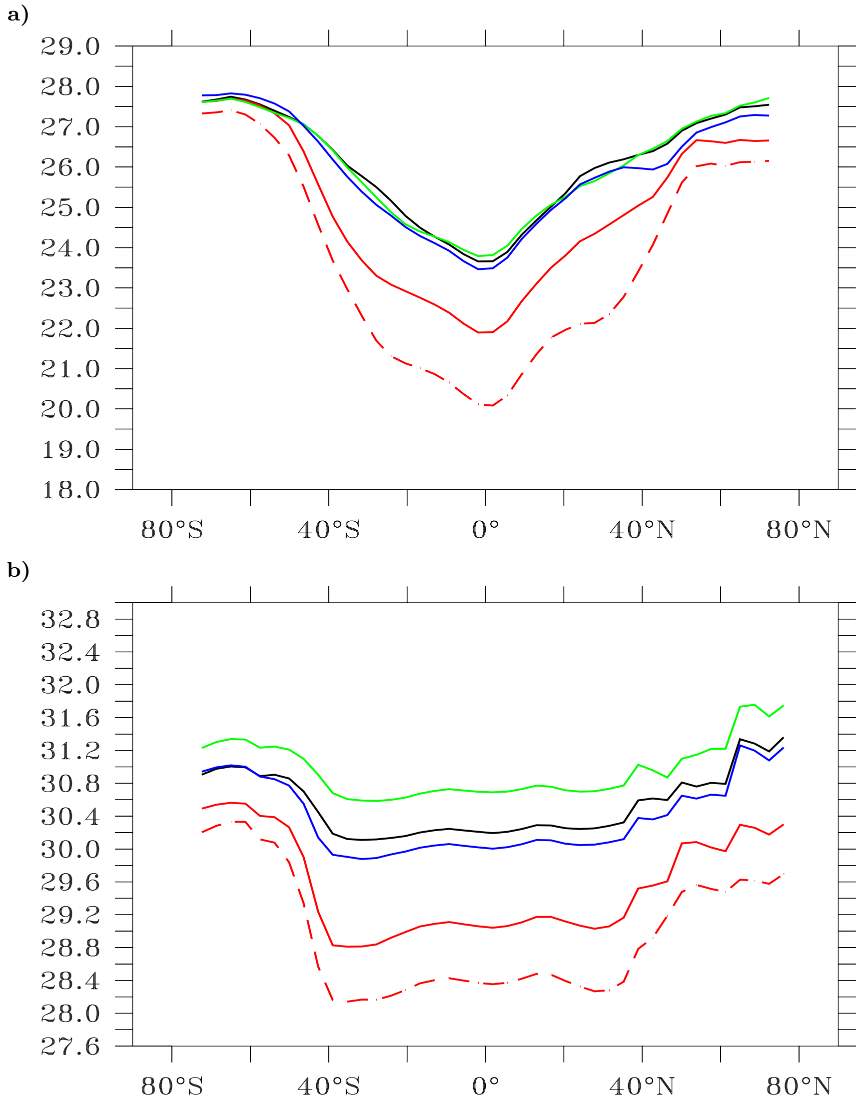

Fig. 4.10: Meridional profiles of the zonal mean of a) surface density and b) depth-integrated density in the Atlantic in different experiments. The lines indicate experiments CLIM (red solid), BH (blue), ABC (black), AC (red dashed) and AB2C (green). Unit is kg/m^3.

stochastic forcing is doubled, this minimum is reduced further (Figure 4.9d).

The above-discussed SST- and SSS-distributions lead to changes in the surface density distribution in the different experiments. The changes in the Atlantic are described by the meridional profiles of zonally averaged surface density in Figure 4.10a. In the mid-latitude South Atlantic, the meridional density gradient is reduced from experiments without the SST-feedback (red solid and red dashed) to experiments BH (blue), ABC (black) and AB2C (green), in which the SST-feedback is included. In the North Atlantic from 50°N to 75°N, the meridional density gradient is weaker in experiments CLIM and AC without the SST-feedback than in experiments BH, ABC and AB2C with the feedback. The situation reverses in the subtropical North Atlantic. Overall, the contrast between surface density in the tropics and in the high-latitude North Atlantic is somewhat larger in experiments without the feedback than in experiments with the feedback.

Comparing the equator-to-pole density contrast with the changes in the Atlantic MOC suggests that a strong contrast is not necessarily related to the strength of the MOC. Experiments CLIM and AC have weak MOC in spite of strong density contrast. In the Southern Ocean, a weaker meridional gradient of the surface density alone does not necessarily produce a weak ACC. Experiment BH has a stronger ACC despite a meridional gradient in the surface density in the southern latitudes that is comparable to experiments ABC and AB2C. This suggests that it is not the changes in the surface density distribution alone which determine the strength of the Atlantic MOC and the ACC.

Indeed the effects of different types of flux anomalies can be traced down to the deep ocean. Figure 4.11 shows the density at 1365 m, which is located, by and large, at the mid-depth of the overturning cell. All density fields are characterized by larger density in the Atlantic and Southern Ocean than in the Pacific and the Indian Ocean. The surface warming in experiment CLIM penetrates into the deep ocean, making the water at 1365 m much lighter in CLIM than that in experiments BH, ABC and AB2C. This is largely corrected by including the SST-feedback. One distinct feature in the North Atlantic is that the isolines are more or less zonally oriented in experiment CLIM (Figure 4.11a), but reveal a notable meridional tilt in experiment BH, ABC and AB2C (Figure 4.11b, c and d). The meridional

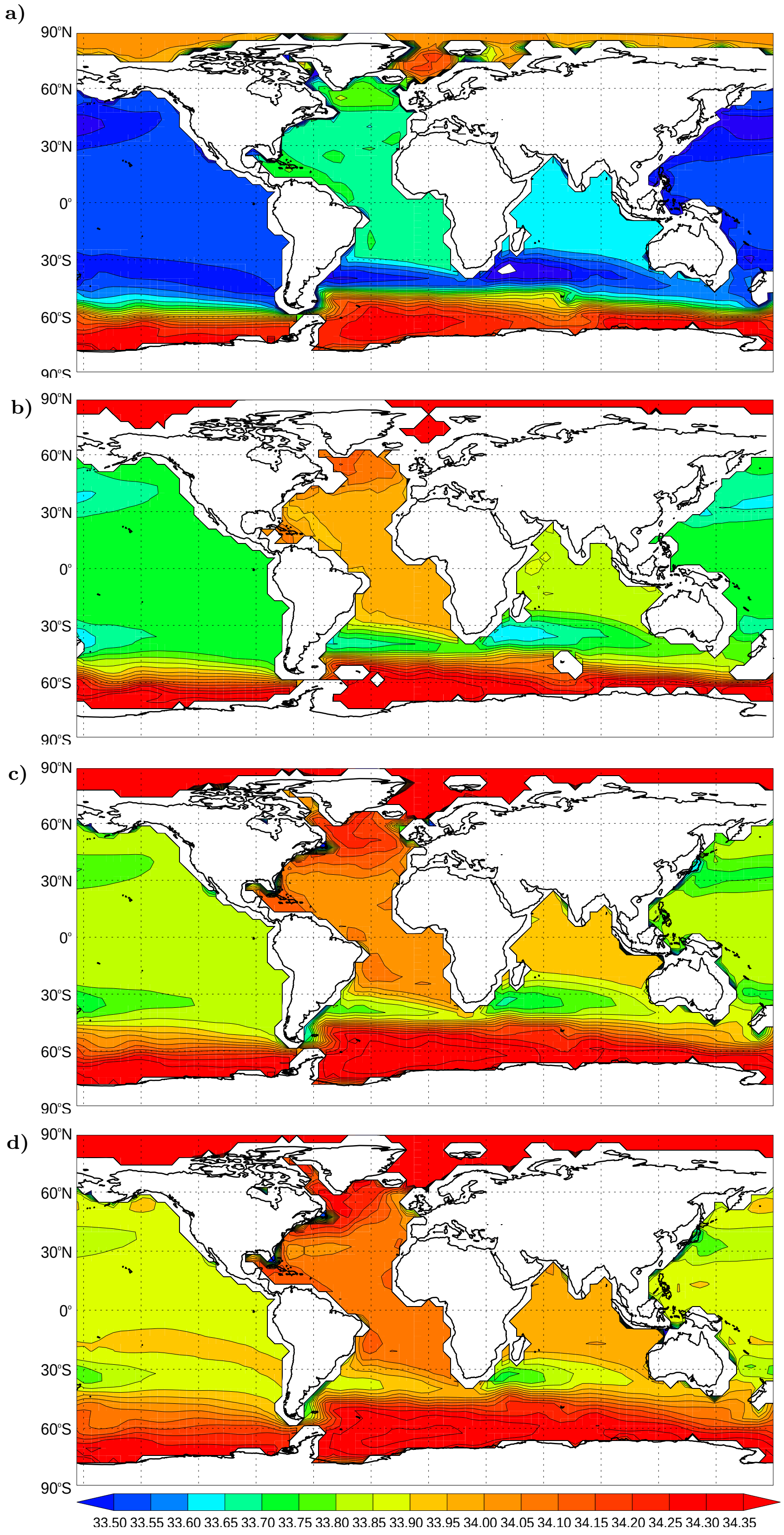

Fig. 4.11: Horizontal distribution of density in kg/m^3 at 1365m in different experiments. a)CLIM, b)BH, c)ABC and d)AB2C.

tilt indicates an increase in the magnitude of the zonal density gradient and hence an increase in the strength of deep, southward flow of the MOC via geostrophic relation. Such a change is consistent with the MOC which increases from experiment CLIM to experiments BH, ABC and AB2C. In the Southern Ocean, there is a reduction in the meridional density gradient from experiment BH without fluctuations in Figure 4.11b to experiments ABC and AB2C with fluctuations in Figure 4.11c and d. This reduction is mainly related to the increase of density near 35°S-40°S.

The density changes in the deep water column is illustrated by the meridional profile of the zonally averaged and depth-integrated density in the Atlantic (Figure 4.10b). The depth integration extends from the surface to the mid-depth of the overturning cell. Despite large changes in the MOC in various experiments, no significant changes in the density gradients are found in the North Atlantic. Generally, it is difficult to relate the meridional density gradient to the strength of the MOC in different experiments. A relationship which stands out is that between the density contrast in the northern and southern high-latitudes and the strength of the MOC. The density is higher in the northern high-latitude Atlantic than in the southern high-latitude Atlantic in the experiments with the SST-feedback (blue, black and green lines in Figure 4.10b) and vice versa in experiment without the SST-feedback (red solid and red dashed lines). A strengthening in this contrast is found to be related to an enhancement in the MOC.

In the Southern Ocean, the magnitude of the meridional density gradient is related to the strength of the ACC. The gradient and the strength of the ACC decreases from experiment AB2C to ABC, BH and finally to CLIM and AC. In contrast to the profile at the surface, there is a clear reduction in the meridional gradient from experiment BH (blue) without fluctuating fluxes to experiments ABC and AB2C with fluctuations (black and green). This reduction is caused by changes induced by fluctuating fluxes as is shown in the next subsection.

4.1.4 Changes in the vertical mixing

One way in which surface fluxes can affect the density in the deep ocean is to change the mixing structure by changing the stratification and velocity shear. Indeed, in this study systematic changes in the mixing structure in the ocean are found in different experiments. In the following, the effects of the flux anomalies on the vertical mixing are identified by considering the difference of K_V in different experiments. The effect of the SST-feedback on the vertical mixing is indicated by the difference BH−CLIM, that of fluctuating fluxes by the difference AC−CLIM, the effects of both oceanic feedbacks and stochastic forcing by the difference ABC−CLIM, and finally the effect of oceanic feedbacks and the enhanced stochastic forcing by the difference AB2C−CLIM.

The differences just listed are obtained by taking CLIM as the control experiment. Apart from these differences, differences obtained by taking experiment BH as the control experiment (i.e. CLIM−BH, ABC−BH and AB2C−BH) were also calculated. When choosing BH as the reference, the effect of SST-feedback is indicated by CLIM−BH (as BH−CLIM but with opposite sign) and the effect of fluctuations by ABC−BH and AB2C−BH. It is found that the fluctuating effect identified from ABC−BH is similar to that identified from AC−CLIM. The following concentrates on differences relative to CLIM for two reasons. First, choosing CLIM as the reference allows a more precise identification of the effect of daily fluxes. This is because $\mathcal{B}$ in the experiments ABC and AB2C contains not only the SST-feedback, but also other oceanic feedbacks. As a result, ABC−BH describes, strictly speaking, the effect of fluctuations plus that of other oceanic feedbacks. Secondly, the difference, ABC−CLIM also allows the identification of the total effect of the daily fluxes (i.e. all feedbacks plus fluctuations), which is impossible when considering ABC−BH.

At 285m depth, the difference BH−CLIM suggests that the SST-feedback enhances the mixing in the mid- and high-latitude oceans (Figure 4.12a). In particular, an increase of K_V of about 0.03 to 0.04 m^2s^{-1} in the entire Southern Ocean from about 30°S to the Antarctic coast is found. Considerable increases are also found in the subtropical North Atlantic, northern North Atlantic, and the northwestern Pacific. In all these areas, reductions in SST from experiment CLIM to BH are found, suggesting that the increase in the K_V is induced by a reduction in the static stability.

The picture is different for changes induced by fluctuations, as shown by the difference AC−CLIM in Figure 4.12b. Both enhancement and reduction of mixing are found outside the tropics in both hemispheres. In the North Atlantic, large-scale increases in K_V are found south of the Greenland-Scotland ridge, while decreases in K_V are found in the northern North Atlantic, leading to a dipole structure in the North Atlantic with a negative center in the GIN Sea. In the Southern Ocean, an increase in K_V is found in the latitude band from 20°S to 55°S. South of this band, negative values of up to -0.03 m^2s^{-1} are found. The bands of positive and negative values form a latitudinal dipole structure with the band of negative values along the Antarctic coast.

Figure 4.12c) shows the result obtained when combining oceanic feedback and stochastic forcing. By and large, the two effects sum up linearly. The latitudinal dipole band in the Southern Ocean is still present. The strengthening of the stochastic forcing further extends the region of enhanced mixing in experiment AB2C (Figure 4.12d).

At 900m depth, the SST-feedback leads again to an enhanced mixing in the Southern Ocean and in the northern North Atlantic (Figure 4.13a).

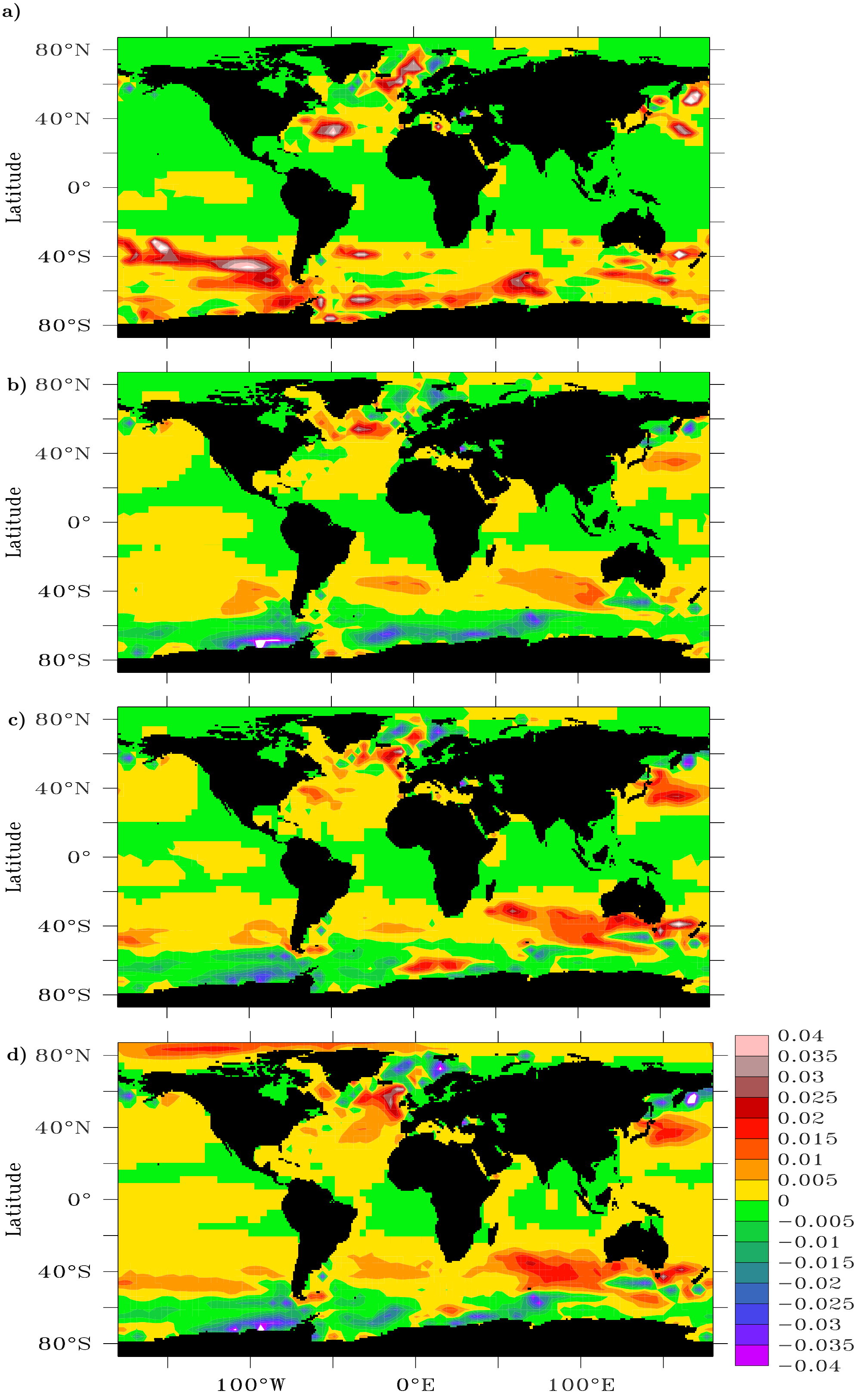

Fig. 4.12: Difference of vertical mixing coefficient, K_V at 285m depth between a)BH and CLIM b)AC and CLIM c)ABC and CLIM d)AB2C and CLIM. Unit is m^2/s.

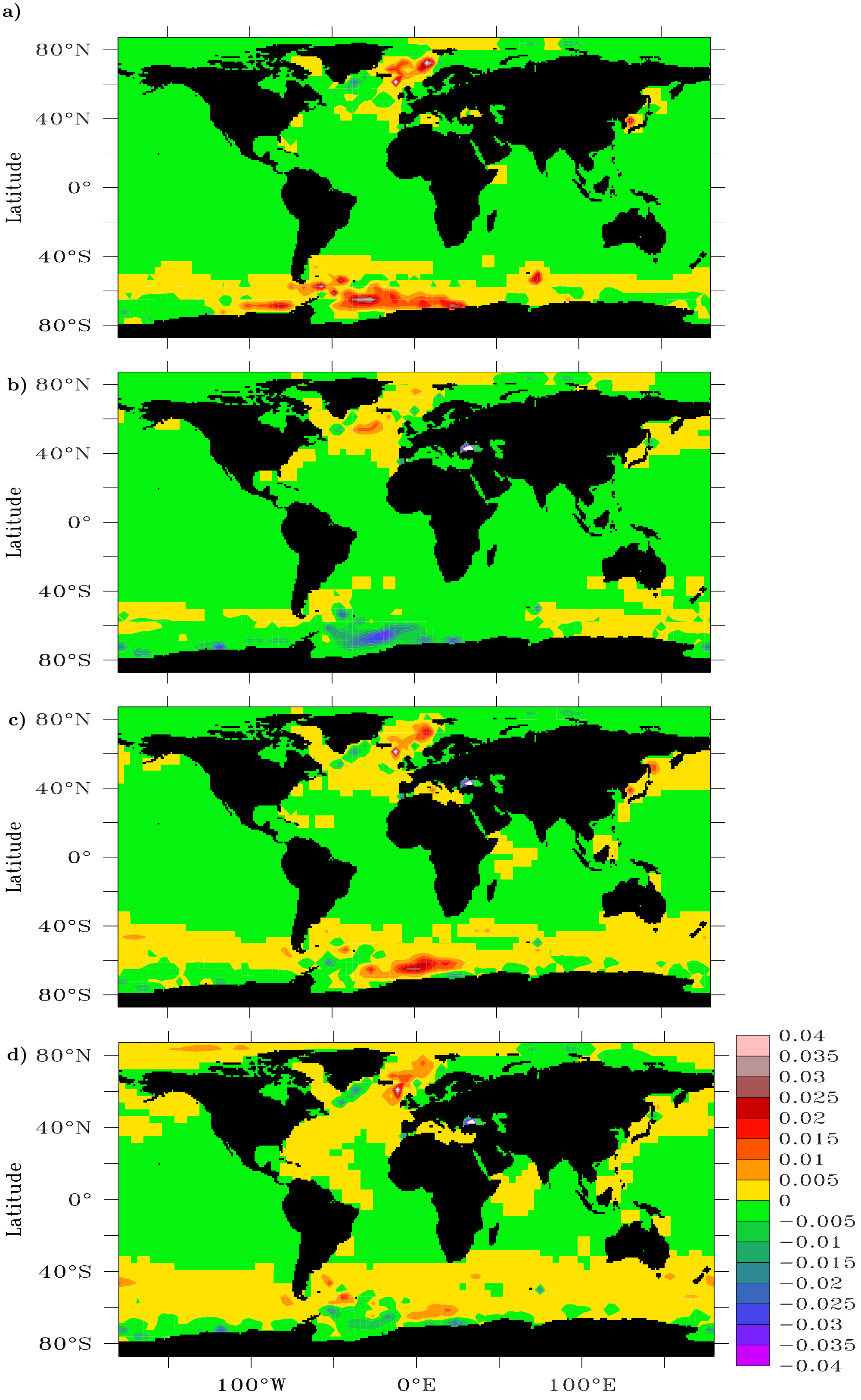

Fig. 4.13: Difference of vertical mixing coefficient, K_V at 900m depth between a)BH and CLIM b)AC and CLIM c)ABC and CLIM d)AB2C and CLIM. Unit is m^2/s.

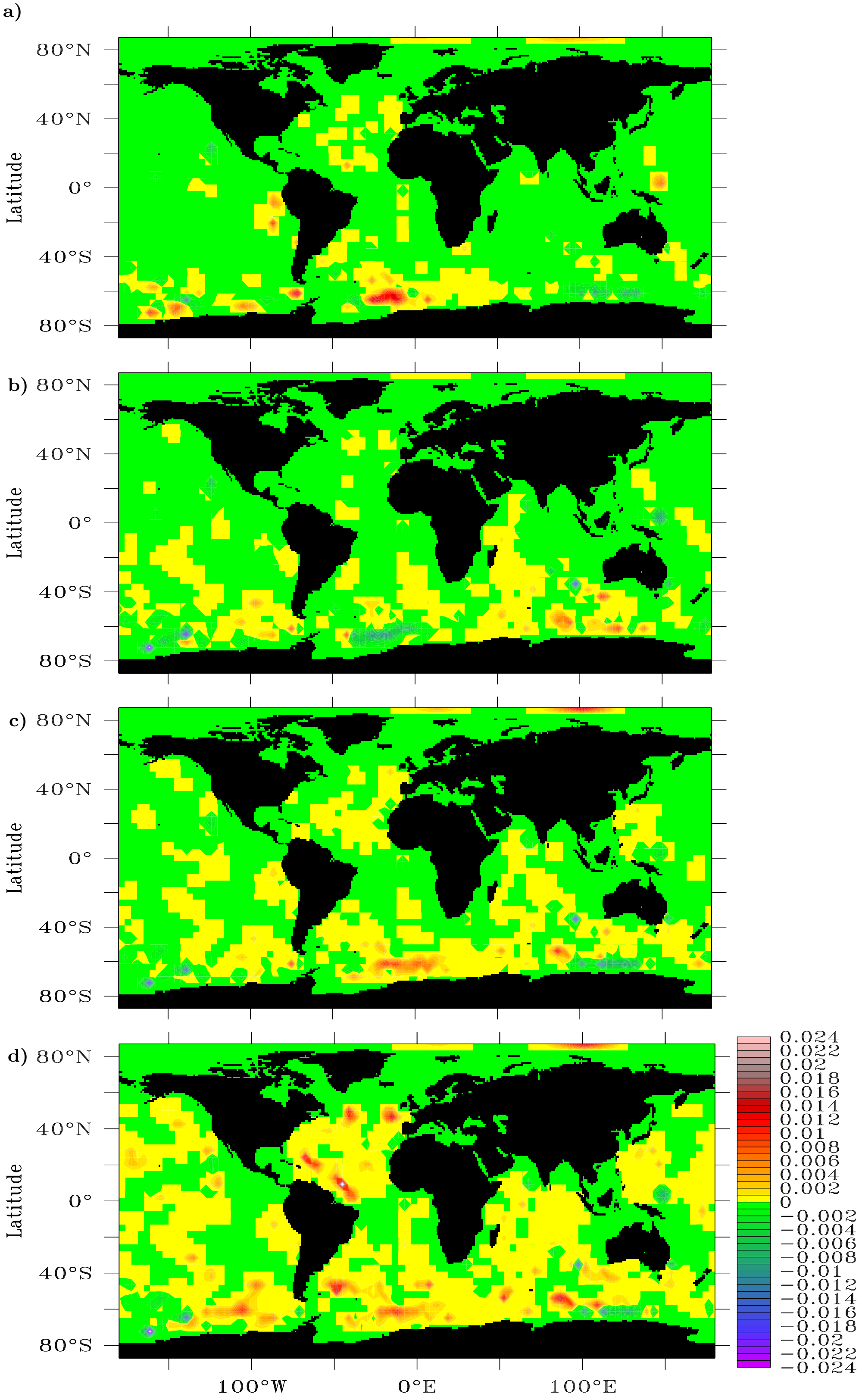

Fig. 4.14: Difference of vertical mixing coefficient, K_V at 3970m depth between a)BH and CLIM b)AC and CLIM c)ABC and CLIM d)AB2C and CLIM. Unit is m^2/s.

There is still some indication of the existence of the latitudinal dipole band in the Southern Ocean which is induced by the fluctuating forcing. However, the dipole structure is much less pronounced at 900m depth (Figure 4.13b) than at 285m depth(Figure 4.12b). In the difference ABC−CLIM (Figure 4.13c), an enhancement of mixing in most of the mid- and high-latitude oceans is found. The mixing maxima in the North Atlantic (Figure 4.13c) consists of the enhancement to the north of the Greenland-Scotland ridge due to the SST-feedback (Figure 4.13a) and the enhancement further to the south due to stochastic forcing (Figure 4.13b). Again, the area with enhanced mixing is significantly enlarged when the stochastic forcing is doubled in experiment AB2C (Figure 4.13d). Mixing structures similar to Figure 4.13 can be found down to depths of about 2500 to 3000 m. Further below, the mixing signal is far less zonally oriented but varies geographically as shown in Figure 4.14. At 3970m depth, the maximum increase in mixing is found in experiment AB2C over the entire Southern Ocean and the abyssal North Atlantic and North Pacific.

The changes in K_V above described, in particular those in the mid- and high-latitude oceans, are to a large extent induced by changes in the convective events. Figure 4.15a shows the difference of the mean convection depth between experiment BH and CLIM. The figure indicates the changes in the mean convection depth due to the SST-feedback. The increase in the mean convection depth in the northern North Atlantic occurs in a statically less stable region, where a reduction in SST due to the SST-feedback leads to further destabilization and hence an increase in convection depth. These changes correspond to the enhanced mixing in the same region in Figure 4.12a and Figure 4.13a.

The difference in the mean convection depth between experiment AC and CLIM shown in Figure 4.15b indicates the changes in the mean convection depth due to fluctuations in the fluxes. The increase in the mean convection

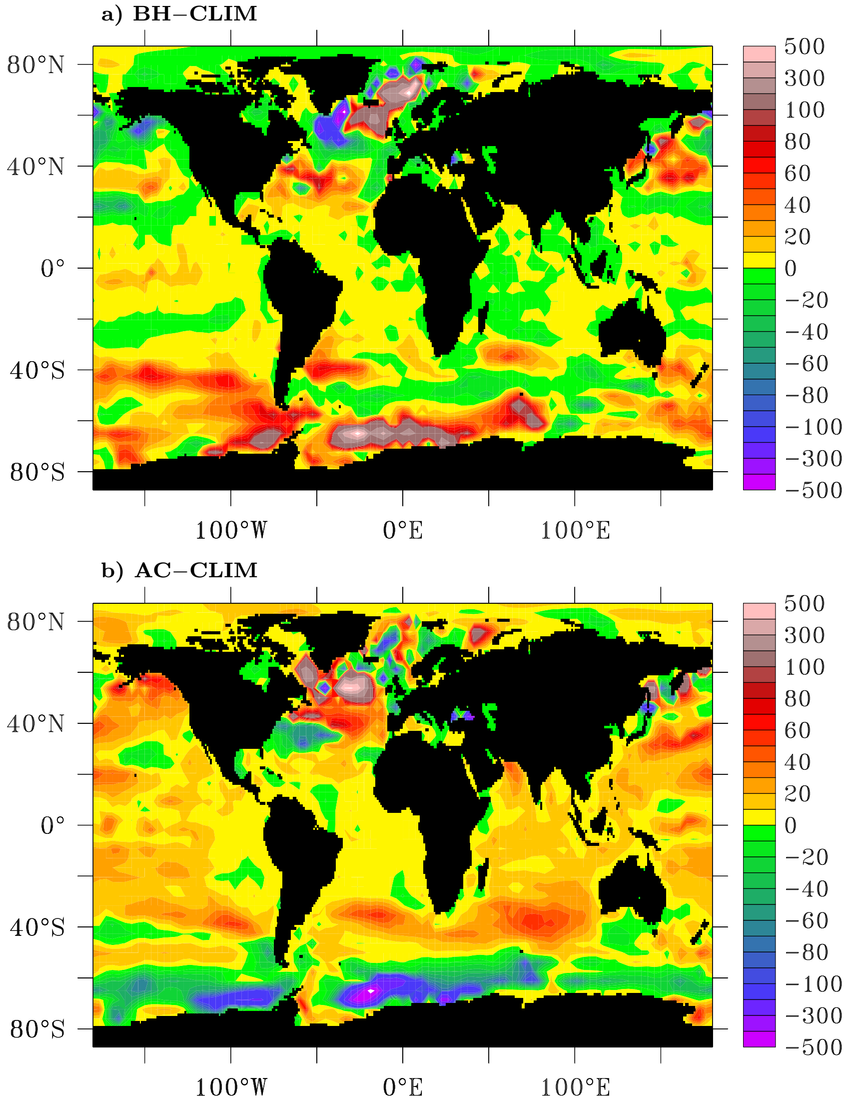

Fig. 4.15: Difference of mean depth of convection in m between a)BH and CLIM and b)AC and CLIM. The shading intervals are uneven (10m in the range -100 to 100m and 100m interval for the rest). Colors are labelled every two interval.

depth in the North Atlantic south of the Greenland–Scotland ridge and the decrease north of it corresponds to the dipole mixing structure in the North Atlantic with the negative center in the GIN Sea in Figure 4.12b. The increase in the mean convection depth in the mid-latitude Southern Ocean and the decrease south of it correspond to the latitudinal dipole structure of the changes in the mixing in the Southern Ocean with the band of negative values along the Antarctic coast which is shown in Figure 4.12b. These changes are consistent with mixing changes induced by fluctuating fluxes because of the non-linear nature of convection. Due to the non-linearity, the fluctuating buoyancy forcing tends to increase the convective mixing over mostly stable ocean regions and to decrease convective mixing over mostly unstable ocean regions. In the MPI-OM model the former is the case in the subtropical oceans, whereas the latter occurs in the GIN Sea and along the Antarctic coast.

The relation of convective activity to the changes in the mixing coefficient K_V at 285m becomes less clear in the tropics and partly in the subtropics. This is because convective events are confined to the upper 60m in the tropical and subtropical Atlantic and to the upper 100m in the tropical and subtropical Pacific, but can reach from a few hundred meters down to a thousand meters or more in the extra-tropics and high-latitudes. Since the convective events triggered by the daily flux anomalies will not reach a deeper layer in the tropics, there is no corresponding change in K_V in the tropics at 285 meter depth as shown in Figure 4.15 and Figure 4.12. The changes in K_V found in the tropical Pacific is likely caused by the *Ri*-dependent mixing, since the increase in depth of convection is confined to about 150m.

4.2 Discussion

The numerical experiments suggest that daily flux anomalies significantly affect the time-mean circulation in the MPI-OM. The following discusses further the exact roles of oceanic feedbacks and of fluctuations of the daily flux anomalies for the MOC and ACC.

4.2.1 Role of the SST-feedback on the MOC

Among all components of the daily fluxes, the SST-feedback is most important for determining the strength of the MOC. This is substantiated by an increase in the MOC of about 3 Sv obtained by switching on the SST-feedback in experiment BH. This increase is notably larger than the further increase of about 1 Sv obtained when other oceanic feedbacks and fluctuations are included in experiment ABC. The SST-feedback affects the MOC by directly setting the correct density distribution at the sea surface and indirectly affecting the density in the deep ocean by changing the stratification and from that the vertical mixing.

Both the SST-feedback and the fluctuations in the daily flux anomalies cause changes in the vertical mixing. These changes are, however, less decisive relative to the SST-feedback. This is suggested by experiment AC, in which oceanic feedbacks are completely switched off. Even though large-scale changes in the vertical mixing are found in AC, the MOC remains weak as in experiment CLIM.

Nevertheless, one cannot completely rule out the role of vertical mixing induced by fluctuating fluxes. Once a realistic density distribution is set by the SST-feedback, the large-scale increase in the vertical mixing in the subtropical ocean (Figure 4.12b and Figure 4.13b) can affect the strength of the MOC. The increase of about 1 SV from BH to ABC is likely due to this large-scale increase in mixing via fluctuating fluxes. Furthermore, since this increase in mixing remains significant in the deep North Atlantic down to depths of about 3500 m, it may also lead to an enhancement of the mixing of North Atlantic Deep Water with Antarctic Bottom Water. Such an enhancement can cause the southward branch of the Atlantic MOC to extend into the deeper layer, leading to a downward extension of the MOC-cell consistent with Figure 4.6e.

4.2.2 Role of fluctuating fluxes on the ACC

In contrast to the MOC, the SST-feedback alone does not affect the strength of the ACC too much. Although there is a reduction in the ACC of about 10 Sv from experiment CLIM to experiment BH by including the SST-feedback, experiment BH still produces an ACC of about 200 Sv, which is too high relative to the observed value of about 120 to 150 Sv (Nowlin and Klinck, 1986 ; Cunningham et al., 2003). A notable weakening of the ACC is only found when additionally fluctuating fluxes are included in experiment ABC. The fluctuations, presumably those in the buoyancy forcing, lead to an increase in convective mixing in the mid-latitude Southern Ocean and a decrease in convective mixing in the Southern Ocean.

The non-linear nature of convection is responsible for these changes: Over the mostly stable mid-latitude Southern Ocean, only negative buoyancy anomalies can change the prevailing stratification, thereby producing an increase in convective activity and vertical mixing. Over the mostly unstable high-latitude Southern Ocean, on the other hand, only positive buoyancy anomalies are able to alter the prevailing stratification, thereby producing a reduction in convective activity and vertical mixing. The resulting latitudinal dipole structure leads to a decrease in meridional density gradient and hence to a reduction in the ACC in experiment ABC.

Though not sufficient, the SST-feedback is necessary. This is suggested by experiment AC in which all oceanic feedbacks are switched off. In the absence of the SST-feedback, a far too strong meridional density gradient is obtained which is even stronger than that found in CLIM. This strong gradient is reflected in the highest global mean SST in experiment AC (Figure 4.1), which results from a greater tropical warming in experiment AC than in experiment CLIM. Such a strong meridional density gradient cannot be reduced effectively by the latitudinal dipole structure in mixing produced by fluctuating fluxes.

4.2.3 Relation between the ACC and the MOC

The experiments show that daily flux anomalies affect both the MOC and the ACC such that a stronger MOC is related to a weaker ACC. The result that the flux anomalies can affect the MOC and the ACC is a direct consequence of the fact that flux anomalies are able to change the global 3-dimensional density distribution. This is done by setting the density distribution via the SST-feedback and by introducing additional mixing via the oceanic feedbacks and the fluctuations in the fluxes. It is also possible that daily fluxes could additionally excite resolved fluctuations in the density flux. This will be discussed in the next subsection.

The inverse relation, i.e. a strong MOC goes together with a weak ACC, is caused at least partly by the increase in the mixing in the subtropical oceans which tends to strengthen the MOC and at the same time weakens the ACC by increasing the density in subtropical oceans, hence decreasing the meridional density gradient in the Southern Ocean. The result that a stronger MOC is related to a weaker ACC does not necessarily rule out the role of the upwelling due to the time-mean wind stress forcing, that suggests a relation of a stronger MOC to a stronger ACC. Since the time-mean wind forcing is unchanged, the present experiments are unable to assess such a role of the time-mean wind forcing.

The changes in the ACC found in this study point however to the baroclinic nature of the ACC caused by the surface bouyancy fluxes and mixing processes. This result is consistent with the work by Olbers et al. (2004) where the dynamics and thermodynamics of the ACC transport is described. In the present experiments, mixing induced by the daily fluxes over the Southern Ocean shows considerable vertical variations in the water column.

Ongoing observational surveys in the Southern Ocean and eddy resolving modeling studies could cast more light into the processes relating MOC and ACC.

4.2.4 Additional role of daily fluxes on resolved fluctuations in the density flux

It has already been shown that the daily fluxes at the surface affect the 3-dimensional density distribution of the ocean by changing the vertical mixing coefficient. The daily fluxes can also change the 3-d density distribution by inducing coherent changes in velocity and density and from that, changes in density fluxes. Concentrating on the vertical density flux, the mean density distribution in the MPI-OM model is described by

$$\frac{\partial \bar{\rho}}{\partial t} + \frac{\partial}{\partial z}(\bar{w}\bar{\rho}) + \frac{\partial}{\partial z}(\overline{w\prime\rho\prime}) + \frac{\partial}{\partial z}\overline{\left(K_V\frac{\partial \rho}{\partial z}\right)} = 0, \qquad (4.1)$$

where $\bar{}$ indicates the time-mean and $w\prime$ and $\rho\prime$ are deviations from the respective mean values.

When driving the ocean with the climatological mean fluxes, as in experiment CLIM, transient variations in $w\prime$ and $\rho\prime$ are negligible. The density distribution is described essentially by the advection and diffusion balance,

$$\frac{\partial}{\partial z}(\bar{w}\bar{\rho}) + \frac{\partial}{\partial z}\overline{\left(K_V\frac{\partial \rho}{\partial z}\right)} = 0 \qquad (4.2)$$

However, when driving the ocean using fluxes including daily fluctuations, the variations in almost all variables are enhanced. Furthermore, if the variations of $w\prime$ and $\rho\prime$ are correlated, i.e. $\overline{w\prime\rho\prime}$ is not zero, one would obtain a non-zero vertical density flux $\overline{w\prime\rho\prime}$ that affects the mean density distribution.

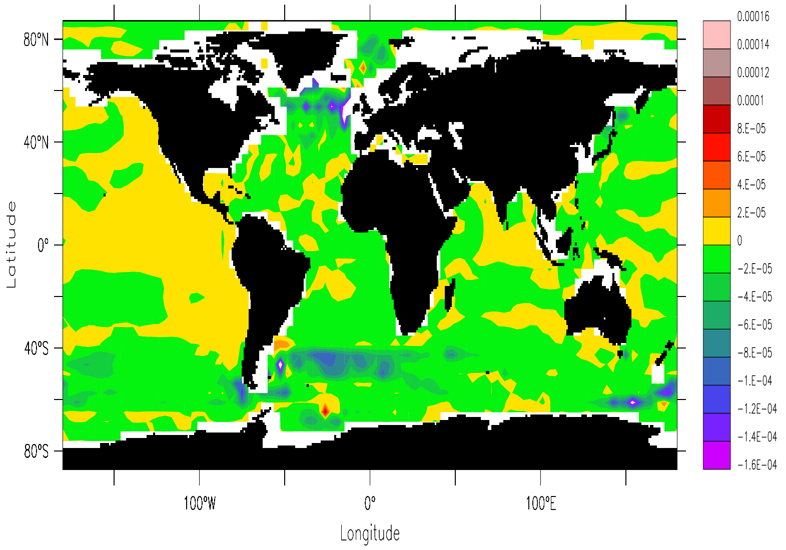

Fig. 4.16: Vertical density flux $\overline{w'\rho'}$ normalised by $|d\overline{\rho}/dz|$ at 1000m in experiment ABC. Unit is m^2/s.

To check whether daily fluxes are indeed able to produce a non-zero vertical density flux, $\overline{w'\rho'}$ at 1000m is calculated from a 50-year-long time slice of the daily data of w and ρ from experiment ABC (Figure 4.16). The flux is normalised by the vertical density gradient $|d\overline{\rho}/dz|$ and hence has the same unit as K_V. Figure 4.16 shows that negative density fluxes occur mainly in the mid-latitude regions of the Atlantic. A negative value of $\overline{w'\rho'}$ indicates downward motion of denser water or upward motion of lighter water. It acts to enhance the prevailing vertical density gradient. The amplitude of $\overline{w'\rho'}$ is, however, two orders of magnitude smaller than that of the changes in K_V, suggesting that the density fluxes induced by fluctuating daily flux anomalies play a negligible role in determining the mean density structure.

5. CONCLUSIONS AND OUTLOOK

This study has demonstrated that the daily surface fluxes is a considerable player in determining the strength of the global meridional overturning circulation. Separate roles of the atmospheric fluctuating part and the oceanic feedback part of the flux anomalies on the time-mean of the ocean have been studied. It is elucidated that both the feedback and the fluctuations contribute to the strength of the MOC. The effect of daily surface flux anomalies is found not only on the time-mean MOC but also on the time-mean Antarctic Circumpolar Current. In addition, it is seen that the strength of the time-mean MOC is inversely related to the strength of the time-mean ACC.

From the discussion and the results of the numerical experiments presented in the previous chapter, the following conclusions can be drawn:

- The surface flux anomalies produce a 4-Sv-increase in the strength of the MOC, which is about 30% of the MOC obtained without the flux anomalies. The increase is caused by changes in the 3-dimensional density structure that are induced by changes in the vertical mixing due to the SST-feedback and fluctuations in the fluxes. The additional mixing due to fluctuating fluxes represents a further mechanism for warming up the deep water which has not been considered so far in the prevailing picture of the MOC outlined in the introduction.

- The strength of the ACC is sensitive to fluctuations in the daily fluxes.

There is a reduction of the ACC of about 65 Sv, which is approximately 30% of the ACC obtained when daily flux anomalies are not taken into account. The reduction is caused by changes in oceanic mixing that is characterized by a meridional dipole of the vertical mixing coefficient in the Southern Ocean induced by fluctuating fluxes.

- A dual effect of fluctuating fluxes, which increases the vertical mixing in mostly stable regions and decreases the vertical mixing in mostly unstable regions, is identified. This effect has not been systematically studied so far.

The above conclusions are drawn within the framework of a coarse resolution version of the MPI-OM. The exact numbers concerning the changes in the MOC and ACC might depend on the model used. Nevertheless, the processes describing how daily flux anomalies change the global density structure should also operate in other models with a similar parameterization of vertical mixing, and probably also in nature.

Outlook

The present study deals with the roles of different types of air-sea fluxes relative to each other, rather than relative to other processes such as the diapycnal mixing through internal waves and the upwelling driven by the time-mean wind stress. It also did not consider the energetics related to the MOC. A possible extension concerning the role of time-mean wind stress is to perform additional experiments with different time-mean wind forcing and compare the results with those from the experiments of this study.

The present study is limited to the effect of daily flux anomalies on the time-mean of the ocean climate system. The effect of flux anomalies on the long-term variability of the ocean is another issue for future investigations. An interesting aspect here is that the excitation of long-term variations through stochastic flux anomalies seem to be strongly limited by the SST-feedback which can be clearly demonstrated using the present experimental set-up.

A further extension of the present study is to explore the effect of the daily fluxes on the sensitivity of MOC to changes in the external forcing, such as an increase in freshwater flux due to the increase in greenhouse-gas concentrations.

6. APPENDIX: MODEL INTEGRATIONS USED TO DERIVE AND VALIDATE EMAD

The parameters $\mathcal{A}$, $\mathcal{B}$ and $\mathcal{C}$ of the EMAD model are derived from a control integration with the ECHO-G AO-GCM (Legutke and Voss, 1999). The atmospheric component is ECHAM-4 and the ocean component is HOPE-G. The resolution of ECHAM4 is T30. For HOPE-G, T42 resolution with equatorial refinement is used. An integration with essentially the same coupled model is discussed by Raible et al. (2001).

To assess the variance produced by the EMAD (section 2.4.2a), EMAD is driven by the SST, sea-ice cover and sea-ice thickness data from ECHAM5/ MPI-OM AO-GCM (Jungclaus et al., 2005). The ECHAM5/MPI-OM model differs from the ECHO-G. The atmospheric component is the ECHAM5 model, rather than the ECHAM4 model. The oceanic component is the MPI-OM formulated on an 'Arakawa C'-grid which has poles over Greenland and Antarctica (Marsland et al. 2003). The oceanic component of the ECHO-G model on the other hand is the HOPE-G model formulated on an 'Arakawa E'-grid. The use of the ECHAM5/MPI-OM integration provides an independent test of EMAD.

To assess the cross-correlation functions (section 2.4.2b), the HOPE-G model (Legutke and Maier-Reimer, 1999) of the same version as that in the ECHO-G model is coupled to the EMAD. The cross-correlation functions calculated from the coupled EMAD/HOPE-G are compared with those obtained from a 50-year-long time slice of ECHO-G integration that was not used to derive the parameters $\mathcal{A}$, $\mathcal{B}$ and $\mathcal{C}$ of the EMAD.

References

Barber, D.G., J.M. Hanesiak, W. Chan and J. Piwowar, 2001: Sea-Ice and Meteorological Conditions in Northern Baffin Bay and the NOW polynya between 1979 and 1996. *Atmosphere-Ocean.,* 39, 343-359.

Beena, B.S. and J.-S. von Storch, 2006: Effect of daily surface flux anomalies on the time-mean circulation in the ocean. *J. Climate.,* (submitted).

Brümmer, B. and D. Schröder, 2002: Temporal and spatial variability of surface fluxes over the ice edge zone in the northern Baltic Sea. *J. Geophy. Res.,* 107, C8, 3096, doi:10.1029/2001JC000884.

Cunningham, S., S. Alderson, B.A. King and M.A. Brandon, 2003: Transport and variability of the ACC. *J. Geophys. Res.,* 108, C5, 8084, doi:10.1029/2001JC001147.

Frankignoul, C., 1985: Sea surface temperature anomalies, planetary waves, and air-sea feedbacks in the middle latitudes. *Rev. Geophy.,* 23, 357-390.

Frankignoul, C., A. Czaja and B. L'Heveder, 1998: Air-sea feedback in the North Atlantic and surface boundary conditions for ocean models. *J. Climate.,* 11, 2310-2324.

Gent, P.R., J. Willebrand, T. McDougall and J.C. McWilliams (1995) Parameterising eddy induced tracer transports in ocean circulation models. *J.Phys. Oceanogr.,* 25, 463-474.

Gregg, M., T. Sanford and D. Winkel, 2003: Reduced mixing from the breaking of internal waves in equatorial waters. *Nature.,* 422, 513-515.

Griffies, S.M., 1998: The Gent-Mc Williams skew flux. *J. Phys. Oceanogr.,* 28, 831-841.

Haak, H., J.H. Jungclaus, U.Mikolajewicz and M. Latif, 2003: Formation and propagation of great salinity anomalies. *Geophys. Res. Lett.,* 30, 1473, doi:10.1029/2003GL017065.

Haney, R.L., 1971: Surface thermal boundary condition for ocean circulation models. *J. Phys. Oceanogr.,* 1, 241-248.

Jungclaus, J.H., H. Haak, M. Latif and U.Mikolajewicz, 2005: Arctic-North Atlantic Interactions and Multidecadal Variability of the Meridional Overturning Circulation. *J. Climate.,* 19, 4016-4034.

Kuhlbrodt, T., A. Griesl, M. Montoya, A. Levermann, M. Hoffmann and S.Rahmstorf, 2006: On the driving processes of the oceanic meridional overturning circulation. *Reviews of Geophys.,* (submitted)

Latif, M., and A. Villwock, 1990: Interannual variability as simulated in coupled ocean-atmosphere models. *J. Mar. Systems.,* 1, 51-60.

Ledwell, J., A. Watson,and C. Law, 1993: Evidence for slow mixing across the pycnocline from an open-ocean tracer release experiment. *Nature.,* 364, 701-703.

Ledwell, J., E. Montgomery, K. Polzin, St.Laurent, L. Schmitt and J. Toole, 2000: Evidence for enhanced mixing over rough topography in the abyssal ocean. *Nature.,* 403, 179-182.

Legutke S., and Voss R, 1999: The Hamburg atmosphere-ocean coupled circulation model ECHO-G. *Technical Report.,* 18, Deutsches Klimarechenzentrum (DKRZ), Hamburg, Germany.

Legutke S., and E. Maier-Reimer, 1999: Climatology of the HOPE-G global ocean-sea ice general circulation model. *Technical Report.,* 21, DKRZ, Hamburg, Germany.

Marotzke, J., 1991: Influence of convective adjustment on the stability of the thermohaline circulation. *J. Phys. Oceanogr.,* 21, 903-907.

Marsland, S.J., H. Haak, J.H. Jungclaus, M. Latif and F. Roeske, 2003: The Max-Planck-Institute global ocean/sea ice model with orthogonal curvilinear coordinates. *Ocean Modell.,* 5, 91-127.

Mikolajewicz, U., and E. Maier-Reimer, 1990: Internal secular variability in an ocean general circulation model. *Climate Dyn.,* 4, 145-156.

Moum, J., D. Caldwell, J. Nash, and G. Gunderson, 2002: Observations of boundary mixing over the continental slope. *J. Phys. Oceanogr.,* 32, 2113-2130.

Munk, W., and C. Wunsch, 1998: Abyssal recipies II. Energetics of tidal and wind mixing. *Deep-Sea Res.,* I, 45, 1977-2010.

Nowlin, W.D.J., and J.M. Klinck, 1986: The physics of the ACC. *Rev. Geophysics.,* 24, 469-491.

Olbers, D., D. Borowski, C. Wolker and J. Wolff, 2004: The dynamical balance, transport and circulation of the ACC. *Antarctic Science.,* 16, 439-470.

Pacanowski, R.C., and S.G.H. Philander, 1981: Parameterisation of vertical mixing in numerical models of tropical oceans. *J. Phys. Oceanogr.,* 11, 1443-1451.

Philander, S. G., 1990: El Niño, La Niña, and Southern Oscillation. Academic Press, San Diago, California. 293.

Polzin, K., J. Toole, J. Ledwell and R. Schmitt, 1981: Spatial variability of turbulent mixing in the abyssal ocean. *Science.,* 276, 93-96.

Rahmstorf, S., 1995: Bifurcations of the Atlantic thermohaline circulation in response to changes in the hydrological cycle. *Nature.,* 378, 145-149.

Rahmstorf, S., and J. Willebrand, 1995: The role of temperature feedback in stabilizing the thermohaline circulation. *J. Phys. Oceanogr.,* 25, 787-805.

Raible, C., U. Luksch, K. Fraedrich, and R. Voss, 2001: North Atlantic decadal regimes in a coupled GCM simulation. *Climate Dynamics.,* 18, 321-330.

Redi, M.H., 1982: Oceanic isopycnal mixing by coordinate rotation. *J. Phys. Oceanogr.,* 12, 1154-1158.

Sandström, J.W., 1908: Dynamische Versuche mit Meerwasser. *Annalen der Hydrographie und der Maritimen Meteorologie.,* 36, 6-23.

Sloyan, B.M., 2005: Spatial variability of mixing in the Southern Ocean. *Geophys. Research Letters.,* 32, L18603, doi:10.1029/2005GL023568.

Sun, De-Zheng, 2003: A possible effect of an increase in the warm pool SST on the magnitude of El Niño warming. *J. Climate.,* 16, 185-205.

Toggweiler, J.R., and B. Samuels, 1993: New radiocarbon constraints on the upwelling of abyssal water to the ocean's surface. *Global Carbon Cycle.,* NATO ASI Series, 303-331.

Toggweiler, J.R., and B. Samuels, 1995: Effect of Drake Passage on the global thermohaline circulation. *Deep-Sea Res.,* 42, 477-500.

UNESCO, 1983: Algorithms for computation of fundamental properties of sea water. *UNESCO Technical Papers in Marine Sciences.,* 44.

Valcke, S., L. Terray and A. Piacentini, 2000: Oasis 2.4, Ocean Atmosphere Sea Ice Soil: User's guide. *CERFACS Technical Report.,* TR/CMGC/03/69, CERFACS, Toulouse, France.

von Storch, J.-S., 2000: Signatures of air-sea interactions in a coupled atmosphere-ocean GCM. *J. Climate.,* 13, 3361-3379.

von Storch, J.-S., J.P. Montavez and B.S. Beena, 2005: EMAD: An empirical model of air-sea fluxes. *Meteorologische Zeitschrift.,* 14, 755-762.

Webb, D.J., and N. Suginohara, 2001: Vertical mixing in the ocean. *Nature.,* 409, 37.

Willebrand, J., 1993: Forcing the ocean by heat and freshwater fluxes. *Energy and Water Cycles in the Climate System.,* NATO ASI Series, NATO, 215-233.

Acknowledgments

First and foremost, I would like to express my deepest gratitude to Dr. Jin-Song von Storch for supervising and encouraging this study. I am thankful to her for always having an open ear to my doubts and also for training me in the art of scientific writing. On a personal note, I thank her for all the friendly advices and guidance throughout the course of this study. I am grateful to Prof. Detlef Quadfasel for reviewing this thesis. Financial support for this study was provided by the SFB-512 project "Cyclones and North Atlantic Climate System", funded by the German Research Foundation. Thanks to the SFB family for the cordial work culture.

I am thankful to Dr. Juan Pedro Montavez for introducing me to the atmospheric model and Dr. Helmuth Haak and Dr. Johann Jungclaus for the technical support and discussions related to the ocean model and coupling. Thanks to Max-Planck Institute for Meteorology for the stimulating work environment and German Climate Computing Centre (DKRZ) for providing the computing facilities. Dr. Rene Redler, NEC, is acknowledged for his friendly attitude and technical help during the beginning of this study. Special thanks to Dr. Dirk Notz for proofreading and helping me with the finishing touches of the thesis.

I deeply acknowledge the suggestions and inspiration from Prof. Hans von Storch and Prof. Peter Müller in the early stages of this study. I am indebted to Prof. Jochem Marotzke for the wednesday group discussions, which were informative and helpful. Special thanks to Dr. Rüdiger Gerdes and Dr. Uwe Mikolajewicz for remarks and suggestions at various stages of this study.

I thank Katja, Julie, Martin, Juergen, Holger, Daniela, Fiona, Dirk, Oliver, Traute, Katja, Trygve, Semeena, Susanne, Stefan, Hans-Stefan, Heiko, Simon, Martina, Frank, Torben, David, Guido, Jayanarayanan, Mon-

alisa, Abhay, Abha, Marion, Viju, Sreerekha, Robin, Johanna, Clotilde, Felix, Peter, Heiko, Mu Lin, Rita, Malte, Gabi, Miren, Torben, Guy, Swagata, Francesca, Marin, Luca, Jose, Luis, Patrice, Nidia, Alvaro, Ingrid, Caroline, Steven, Anita, Xiuhua, Manik, Manu, Philip, Tatjana and Melissa for their care, humour and friendship. Thanks to my hostel friends Claudi, Daniel, Pedro, Priya, Frauke, Kristof, Sara, Katja and Marcus who made my stay pleasant. Fidel and his friends are acknowledged for making the short stay at Universidad Complutense de Madrid enjoyable.

I recall with gratitude the encouragement from my teachers and friends at CUSAT, NIO and IISc to start my PhD study. I am grateful to Smitha, Aniyettan, Suchithra, Sukesh, Madhu Annan, Arindam, Anitha, Retish, Prince, Francis, Nomi, Lavanya, Teji and Alljayans who made me cheerful with their overseas-friendship. I cannot forget the medical doctors and sports teachers in Hamburg who helped me overcome the RSI.

I am indebted to my parents and in-laws, Shaji Annan, Sheeja, Reji, Athira and uncle Uthaman for supporting my wishes and encouraging me to get ahead in life. Finally, I dedicate this thesis to Hari for always holding my hands.

Publikationsreihe des MPI-M
„Berichte zur Erdsystemforschung“ , „*Reports on Earth System Science*“, ISSN 1614-1199
Sie enthält wissenschaftliche und technische Beiträge, inklusive Dissertationen.

Berichte zur Erdsystemforschung Nr.1 Juli 2004	**Simulation of Low-Frequency Climate Variability in the North Atlantic Ocean and the Arctic** Helmuth Haak
Berichte zur Erdsystemforschung Nr.2 Juli 2004	**Satellitenfernerkundung des Emissionsvermögens von Landoberflächen im Mikrowellenbereich** Claudia Wunram
Berichte zur Erdsystemforschung Nr.3 Juli 2004	**A Multi-Actor Dynamic Integrated Assessment Model (MADIAM)** Michael Weber
Berichte zur Erdsystemforschung Nr.4 November 2004	**The Impact of International Greenhouse Gas Emissions Reduction on Indonesia** Armi Susandi
Berichte zur Erdsystemforschung Nr.5 Januar 2005	**Proceedings of the first HyCARE meeting, Hamburg, 16-17 December 2004** Edited by Martin G. Schultz
Berichte zur Erdsystemforschung Nr.6 Januar 2005	**Mechanisms and Predictability of North Atlantic - European Climate** Holger Pohlmann
Berichte zur Erdsystemforschung Nr.7 November 2004	**Interannual and Decadal Variability in the Air-Sea Exchange of CO2 - a Model Study** Patrick Wetzel
Berichte zur Erdsystemforschung Nr.8 Dezember 2004	**Interannual Climate Variability in the Tropical Indian Ocean: A Study with a Hierarchy of Coupled General Circulation Models** Astrid Baquero Bernal
Berichte zur Erdsystemforschung Nr9 Februar 2005	**Towards the Assessment of the Aerosol Radiative Effects, A Global Modelling Approach** Philip Stier
Berichte zur Erdsystemforschung Nr.10 März 2005	**Validation of the hydrological cycle of ERA40** Stefan Hagemann, Klaus Arpe and Lennart Bengtsson
Berichte zur Erdsystemforschung Nr.11 Februar 2005	**Tropical Pacific/Atlantic Climate Variability and the Subtropical-Tropical Cells** Katja Lohmann
Berichte zur Erdsystemforschung Nr.12 Juli 2005	**Sea Ice Export through Fram Strait: Variability and Interactions with Climate**- Torben Königk
Berichte zur Erdsystemforschung Nr.13 August 2005	**Global oceanic heat and fresh water forcing datasets based on ERA-40 and ERA-15** Frank Röske
Berichte zur Erdsystemforschung Nr.14 August 2005	**The** HAM**burg** O**cean** C**arbon** C**ycle Model HAMOCC5.1 - Technical Description Release 1.1** Ernst Maier-Reimer, Iris Kriest, Joachim Segschneider, Patrick Wetzel
Berichte zur Erdsystemforschung Nr.15 Juli 2005	**Long-range Atmospheric Transport and Total Environmental Fate of Persistent Organic Pollutants - A Study using a General Circulation Model** Semeena Valiyaveetil Shamsudheen

Publikationsreihe des MPI-M
„Berichte zur Erdsystemforschung“ , „*Reports on Earth System Science*“, ISSN 1614-1199
Sie enthält wissenschaftliche und technische Beiträge, inklusive Dissertationen.

Berichte zur **Erdsystemforschung Nr.16** Oktober 2005	**Aerosol Indirect Effect in the Thermal Spectral Range as Seen from Satellites** Abhay Devasthale
Berichte zur **Erdsystemforschung Nr.17** Dezember 2005	**Interactions between Climate and Land Cover Changes** Xuefeng Cui
Berichte zur **Erdsystemforschung Nr.18** **Januar 2006**	**Rauchpartikel in der Atmosphäre: Modellstudien am Beispiel indonesischer Brände** Bärbel Langmann
Berichte zur **Erdsystemforschung Nr.19** **Februar 2006**	**DMS cycle in the ocean-atmosphere system and its response to anthropogenic perturbations** Silvia Kloster
Berichte zur **Erdsystemforschung Nr.20** **Februar 2006**	**Held-Suarez Test with ECHAM5** Hui Wan, Marco A. Giorgetta, Luca Bonaventura
Berichte zur **Erdsystemforschung Nr.21** **Februar 2006**	**Assessing the Agricultural System and the Carbon Cycle under Climate Change in Europe using a Dynamic Global Vegetation Model** Luca Criscuolo
Berichte zur **Erdsystemforschung Nr.22** **März 2006**	**More accurate areal preciption over land and sea, APOLAS Abschlussbericht** K. Bumke, M. Clemens, H. Graßl, S. Pang, G. Peters, J.E.E. Seltmann, T. Siebenborn, A. Wagner
Berichte zur **Erdsystemforschung Nr.23** **März 2006**	**Modeling cold cloud processes with the regional climate model REMO** Susanne Pfeifer
Berichte zur **Erdsystemforschung Nr.24** **Mai 2006**	**Regional Modeling of Inorganic and Organic Aerosol Distribution and Climate Impact over Europe** Elina Marmer
Berichte zur **Erdsystemforschung Nr.25** **Mai 2006**	**Proceedings of the 2nd HyCARE meeting, Laxenburg, Austria, 19-20 Dec 2005** Edited by Martin G. Schultz and Malte Schwoon
Berichte zur **Erdsystemforschung Nr.26** **Juni 2006**	**The global agricultural land-use model KLUM – A coupling tool for integrated assessment** Kerstin Ellen Ronneberger
Berichte zur **Erdsystemforschung Nr.27** **Juli 2006**	**Long-term interactions between vegetation and climate -- Model simulations for past and future** Guillaume Schurgers
Berichte zur **Erdsystemforschung Nr.28** **Juli 2006**	**Global Wildland Fire Emission Modeling for Atmospheric Chemistry Studies** Judith Johanna Hoelzemann
Berichte zur **Erdsystemforschung Nr.29** **November 2006**	**CO_2 fluxes and concentration patterns over Eurosiberia: A study using terrestrial biosphere models and the regional atmosphere model REMO** Caroline Narayan

Publikationsreihe des MPI-M
„Berichte zur Erdsystemforschung“ , „*Reports on Earth System Science*“, ISSN 1614-1199
Sie enthält wissenschaftliche und technische Beiträge, inklusive Dissertationen.

Berichte zur Erdsystemforschung Nr.30 **November 2006**	**Long-term interactions between ice sheets and climate under anthropogenic greenhouse forcing Simulations with two complex Earth System Models** Miren Vizcaino

ISSN 1614-1199